Multi-Scale Modeling of HIV Infection *in vitro* and APOBEC3G-Based Anti-Retroviral Therapy

Iraj Hosseini, Feilim Mac Gabhann*

Institute for Computational Medicine and Department of Biomedical Engineering, Johns Hopkins University, Baltimore, Maryland, United States of America

Abstract

The human APOBEC3G is an innate restriction factor that, in the absence of Vif, restricts HIV-1 replication by inducing excessive deamination of cytidine residues in nascent reverse transcripts and inhibiting reverse transcription and integration. To shed light on impact of A3G-Vif interactions on HIV replication, we developed a multi-scale computational system consisting of intracellular (single-cell), cellular and extracellular (multicellular) events by using ordinary differential equations. The single-cell model describes molecular-level events within individual cells (such as production and degradation of host and viral proteins, and assembly and release of new virions), whereas the multicellular model describes the viral dynamics and multiple cycles of infection within a population of cells. We estimated the model parameters either directly from previously published experimental data or by running simulations to find the optimum values. We validated our integrated model by reproducing the results of *in vitro* T cell culture experiments. Crucially, *both* downstream effects of A3G (hypermutation and reduction of viral burst size) were necessary to replicate the experimental results *in silico*. We also used the model to study anti-HIV capability of several possible therapeutic strategies including: an antibody to Vif; upregulation of A3G; and mutated forms of A3G. According to our simulations, A3G with a mutated Vif binding site is predicted to be significantly more effective than other molecules at the same dose. Ultimately, we performed sensitivity analysis to identify important model parameters. The results showed that the timing of particle formation and virus release had the highest impacts on HIV replication. The model also predicted that the degradation of A3G by Vif is not a crucial step in HIV pathogenesis.

Competing Interests: The authors have declared that no competing interests exist.

* E-mail: feilim@jhu.edu

Introduction

Over the past decade, some human innate restriction factors have been found to attenuate viral replication. These restriction factors, including human APOBEC3G (apolipoprotein B mRNA editing enzyme, catalytic polypeptide-like 3G, or A3G), a potent inhibitor of human immunodeficiency virus type 1 (HIV-1) infection, have been extensively reviewed in [1–6] among others. A3G, a member of the APOBEC family, counteracts retroviral infection primarily by hypermutating retroviral cDNA and by inhibition of viral reverse transcription and integration. In a HIV-infected cell, A3G produced by the cell is encapsulated in progeny HIV-1 particles by binding to the viral RNA genome. When these viruses are released and infect another cell, A3G causes excessive C-to-U deamination of the minus strand DNA during reverse transcription [7–11]. This results in G-to-A hypermutations in the plus strand cDNA [7–9,12], with a mutational frequency of over 10% [2,13]. It has also been proposed that uracil-DNA glycosylases, such as UNG2 or SMUG1 may trigger degradation of uracilated minus strand DNA [14,15]. But, some reports showed that uracil DNA glycosylases do not contribute to antiviral activity of A3G [16–18].

It has been suggested that hypermutation may not be the only A3G activity that restricts HIV replication [19,20]. Deaminase-independent activities of A3G include, but are not limited to, inhibiting synthesis of viral cDNA by blocking translocation of reverse transcriptase along the template RNA [21–23], reduction in the ability of tRNA^{Lys3} primers to initiate reverse transcription [24,25], blocking integration of the double-stranded viral DNA by causing defects in cleavage of tRNA^{Lys3} primer [18], or inhibiting nuclear import of pre-integration complex [26]. Although there is mounting evidence for deaminase-independent activities of A3G, several reports have suggested that these activities are the results of over-expression of A3G in cells [27–29]. As mentioned, A3G normally mediates antiviral activities in the target cells after being packaged in the newly budded viruses from the virus-producing cells. Evidence supporting this observation came from studies performed almost 10 years before discovery of A3G [30–32]. Recently, Chiu *et al.* have shown that A3G may also restrict HIV-1 infection in resting CD4+ T cells [33]; however, other groups could not verify this phenomenon [34,35]. Further investigation is required to illuminate the new potential mechanisms of A3G against HIV-1.

HIV-1 is a retrovirus, more specifically a lentivirus. It encodes nine genes, of which *gag*, *pol* and *env* are common to all retroviruses. The remaining 6 genes (*tat*, *rev*, *vif*, *vpr*, *vpu* and *nef*) encode proteins with accessory and/or regulatory roles crucial to HIV pathogenesis [36,37]. Viral infectivity factor (Vif), a 23-kDa protein, has an important function in HIV infectivity by inhibiting A3G. It is thought that Vif's primary mechanism of action is to

Author Summary

According to UNAIDS (The Joint UN Programme on HIV/AIDS) and WHO, HIV/AIDS has killed more than 25 million people worldwide since its recognition in 1981. Recently, APOBEC3G, a member of the APOBEC family, has been shown to be a potent inhibitor of HIV infection. In contrast, a viral protein, called Vif, is known to protect the virus by binding to APOBEC3G and causing the degradation of this enzyme. We have developed a computational model to simulate *in vitro* experiments that include A3G-Vif interactions at the intracellular level and T cell-HIV dynamics at the multicellular level. Experimental data were used to establish system parameters and also to validate predictions of our models. We studied various drugs targeting APOBEC3G and Vif pathways to find the optimum therapeutic approach against HIV replication. Our model predicted that a mutated form of APOBEC3G that does not bind to Vif performs significantly better at suppressing HIV replication compared to other drugs. We also found that the drug should be administered shortly after infection and it must be available to all cells in order to be effective.

deplete the intracellular pool of A3G by inducing polyubiquitylation and eventual degradation of A3G through the proteasomal pathway [11,38–41]. Recently, it has been shown that A3G N terminal is a target of Vif-induced polyubiquitylation [42]. However, some evidence suggests that Vif more directly impedes A3G incorporation into HIV-1 virions [12,43]. Sequence analysis studies have shown that an Asp-Pro-Asp motif at positions 128–130 in A3G is crucially important for binding of Vif to A3G. The D128K mutation in A3G protects the protein from Vif-induced degradation [12,44,45]. Mutations at Tyr-124 or Trp-127 make the protein unable to bind viral RNA and therefore get packaged into viruses [46–48]. The 124–127 motif is located beside the 128–130 Vif-binding region in the 3D model structure of A3G shown in Fig. 1A [47]. This suggests that Vif binding and RNA binding may be in competition.

Mathematical models have proven valuable in understanding the dynamics of HIV-1 infection *in vivo* [49]. In most existing HIV infection models, subcellular events such as viral genome replication and integration, production of viral proteins, and release of new virions are often not explicitly reflected [50–56]. Instead, these extracellular models consider several cycles of infection where a population of cells can be infected by viruses and the effects of drug therapies on the number of viruses are studied. By contrast, intracellular models assuming only a single cycle of infection have been limited to the study of the kinetics of virus and host proteins and their interactions to understand the dynamics of viral replication inside the cells [57,58]. Both types of modeling give insights into how HIV disease progresses in the body, however, combining intracellular and extracellular models would greatly enhance our understanding in this area [59].

In our previous work [60], we used a model of a single cell that could undergo multiple re-infection as a surrogate for multicellular infection, to capture both intracellular and extracellular properties of HIV infection. In the present study, we have developed a multiscale system integrating intracellular, cellular and extracellular processes. This integrated model explicitly includes concepts such as burst size (the number of viruses released by a cell), proliferation rate of cells, cell life cycle, virus clearance, and intracellular delays in viral formation and release from cells, which were not explicitly described in the previous model. The integrated model is used to simulate *in vitro* T cell HIV infection experiments.
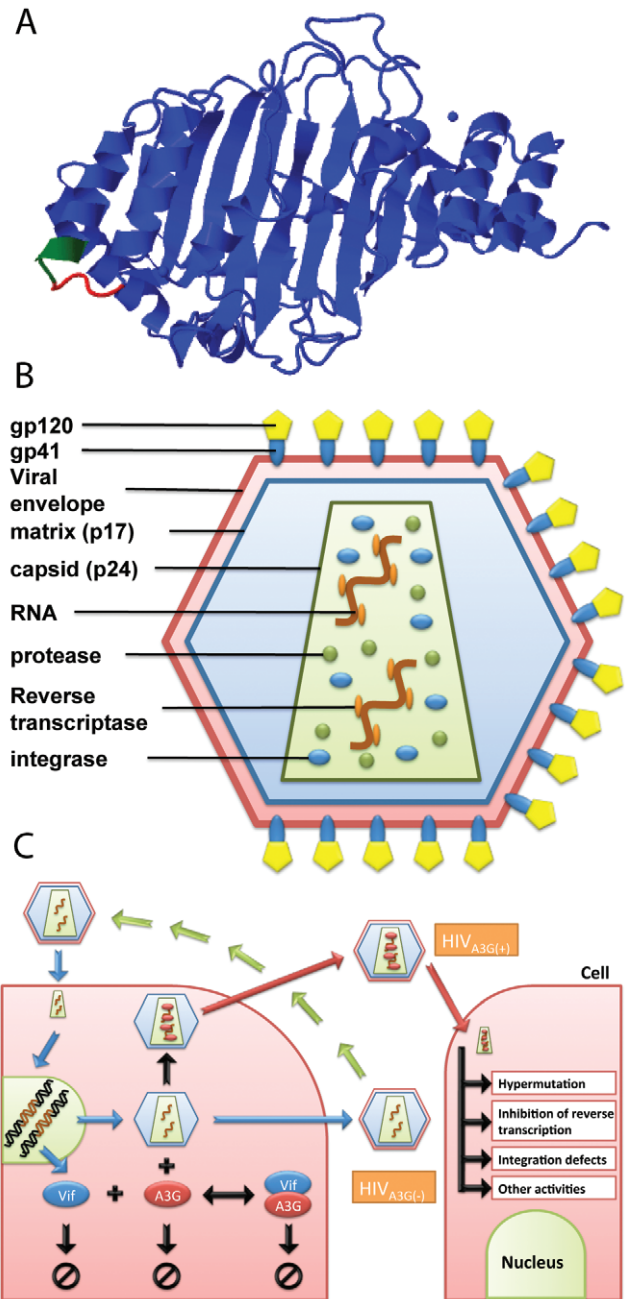

Figure 1. APOBEC3G 3D model structure, HIV virion and its life cycle. (A) 3D model structure of A3G proposed by Zhang *et al.* [47]. The 124–127 motif (red) is located beside the 128–130 Vif-binding region (green). (B) HIV particles are surrounded by fatty materials known as the viral envelope. The matrix formed from p17 protein is another layer underneath the viral envelope. The particles also contain two exact copies of RNA strands as well as three essential enzymes required for replication: reverse transcriptase, integrase and protease. (C) Mechanism of HIV infection including viral entry, genome integration, production and release of new viral particles, and encapsulation of A3G into virions is schematically shown. If the released viruses carry A3G, they are denoted A3G(+) viruses, otherwise they are denoted A3G(−). When A3G(+) viruses infect the next cell, the packaged A3G has several activities such as hypermutating the minus strand of viral DNA, and inhibiting various steps of reverse transcription and integration. "Null" symbols inside the cell represent degradation of Vif, A3G, and A3G-Vif complex.
doi:10.1371/journal.pcbi.1002371.g001

The intracellular (single-cell) model includes interactions between Vif, virus RNA and human A3G. Experimental data are used to establish system parameters such as degradation rate constants of proteins, life-span of infected cells, and viral generation time. The intracellular model sheds light on how changes in the intracellular parameters affect the production and release of new HIV viruses. The single-cell model results are integrated into a multicellular model to simulate T cell culture experiments. We estimate certain parameters such as viral burst size, HIV infectivity rate, and virus clearance rate using experimental data, and model predictions are verified using previously published experimental results. Biologically relevant levels of host and virus proteins in experiments are estimated using our multi-scale system. We monitor how the population of cells acts in response to virus infection. Several drugs targeting A3G and Vif pathways are studied to compare their efficacy at different doses. We also estimate drug efficacy under non-ideal conditions, such as when it is available to only a specific fraction of cells in the whole population, or delivered at later times following infection.

Methods

HIV Biology and System Model

HIV particles are surrounded by a fatty membrane known as the viral envelope. There is another layer underneath the viral envelope called matrix which is formed from p17 protein. HIV has three essential enzymes required for replication: reverse transcriptase, integrase and protease. These enzymes along with two exact copies of RNA strands are packaged in the viral core or capsid. This is also where the A3G is encapsulated into the virus. The viral core is made from the protein p24. A generic structure of HIV virus is shown in Fig. 1B.

Fig. 1C shows the schematic model of HIV infection that is used to develop the computational model, capturing both intracellular and extracellular information. Each cycle of infection begins with a HIV virus attacking a healthy normal cell. After the virus entry into cells, the HIV genome is reverse transcribed into cDNA [61]. Some evidence suggests that HIV capsid remains intact during reverse transcription and that uncoating occurs at the nuclear pore upon completion of reverse transcription, reviewed in [62]. The resulting double-stranded DNA enters the nucleus along with the viral integrase, which splices the HIV DNA into the human genome. The integrated viral DNA, called provirus, is then transcribed into messenger RNA used as a blueprint for making new HIV proteins and enzymes. Some of the viral RNA remains as full-length RNA copies, to be incorporated as viral genetic material for new virions. We model the mechanisms from virus entry to viral protein production using relevant kinetics and intracellular delay parameters. The focus of this study is the interaction between Vif and A3G, and their productions are explicitly included in our model.

HIV enzymes, structural proteins, and full-length RNA molecules are assembled into virions at the cell membrane. Human T cells can produce A3G as an intrinsic defense mechanism. This protein binds the viral RNA and gets encapsidated into the viral capsids while they are still inside the cell. Shortly after viral assembly, the viruses get released from the cells and they are ready to infect new cells. In our model, if the released viruses carry A3G, they are denoted A3G(+) viruses, otherwise they are denoted A3G(−). The encapsulated A3G is assumed to not have effects on viral entry. This is simply because the entry process involves the binding of CD4 and chemokine coreceptors on the T cell surface to gp41 and gp120 on the viral envelope whereas A3G is encapsulated inside the capsid and

doesn't interact with the proteins on the viral envelope. When A3G(+) viruses infect the next cell, the packaged A3G can have various anti-retroviral activities. In this paper, we focus on two downstream effects of A3G; 1) hypermutation in the minus strand of viral DNA; and 2) inhibition of viral cDNA production. This means that even though A3G(+) viruses can infect cells with similar rate of infectivity to A3G(−) viruses, infected cells produce fewer virions. HIV has evolved to combat A3G with Vif. The Vif protein binds A3G and facilitates its polyubiquitylation, and therefore increases its degradation rate. This Vif-induced degradation, and basal rates of degradation of both Vif and A3G, are included in the model. Note that we assume A3G doesn't affect replication of viruses in the producer cell. This has been observed in [30–32] and can be explained assuming that reverse transcription occurs inside the capsid and A3G doesn't have access to transcripts. The single-cell and multicellular models of HIV infection are described using differential equations.

Mathematical Model Development for Intracellular Interactions ("Single-Cell Model")

Our model includes both proteins and virions in a generic human T cell. There is a differential equation for each entity, which describes its production, degradation, and interactions with other entities.

The A3G protein can be produced, degraded, and incorporated into progeny viruses. It also binds to and dissociates from Vif.

$$\frac{d[A3G]}{dt} = P_{A3G} - k_{d,A3G}[A3G] - k_{on}[Vif][A3G] + k_{off}[A3G.Vif] \\ - k_{A3G.HIV}s_{A3G}\{HIV_{(-)}\}[A3G], \tag{1}$$

where P_{A3G} is the production rate of A3G, $k_{d,A3G}$ is the degradation coefficient of A3G, k_{on} and k_{off} are the binding and dissociation constants of the A3G-Vif complex, and $k_{A3G.HIV}$ is the rate constant for A3G incorporation into A3G(−) HIV viruses, denoted by $HIV_{(-)}$. The stoichiometry of A3G proteins incorporated into virions is s_{A3G}. Similarly, Vif concentration is governed by

$$\frac{d[Vif]}{dt} = P_{Vif} - k_{d,Vif}[Vif] - k_{on}[Vif][A3G] + k_{off}[A3G.Vif], \tag{2}$$

where P_{Vif} and $k_{d,Vif}$ are the production rate and the degradation coefficient of Vif, respectively. The A3G-Vif complex can be formed from Vif binding to A3G or it can degrade.

$$\frac{d[A3G.Vif]}{dt} = -k_{d,A3G.Vif}[A3G.Vif] + \\ k_{on}[Vif][A3G] - k_{off}[A3G.Vif], \tag{3}$$

In (3), the degradation coefficient of A3G-Vif complex is shown by $k_{d,A3G.Vif}$. The number of HIV virions inside the cell is also modeled by

$$\frac{d\{HIV_{(-)}\}}{dt} = P_{HIV} - k_{A3G.HIV}\{HIV_{(-)}\}[A3G] - k_{rel}\{HIV_{(-)}\} \tag{4}$$

Viruses are produced at a rate of P_{HIV} and budded off from the cell by a rate of k_{rel}. The A3G protein can get encapsulated into A3G(−) viruses and convert them to A3G(+) viruses. The number of intracellular A3G(+) viruses is governed by

$$\frac{d\{HIV_{(+)}\}}{dt} = k_{A3G.HIV}\{HIV_{(-)}\}[A3G] - k_{rel}\{HIV_{(+)}\}, \tag{5}$$

where $HIV_{(+)}$ refers to A3G(+) viruses. Finally, the release of newly-made HIV viruses is described by the following equations.

$$M_{(-)}(t) = \frac{d\{HIV_{\text{rel},(-)}\}}{dt} = k_{\text{rel}}\{HIV_{\text{rel},(-)}\}, \qquad (6a)$$

$$M_{(+)}(t) = \frac{d\{HIV_{\text{rel},(+)}\}}{dt} = k_{\text{rel}}\{HIV_{\text{rel},(+)}\}. \qquad (6b)$$

In equation (6), $HIV_{\text{rel},(-)}$ and $HIV_{\text{rel},(+)}$ represent released A3G(−) and A3G(+) viruses, respectively. $M_{(-)}(t)$ and $M_{(+)}(t)$, the number of released A3G(−) and A3G(+) viruses at time t, will be used later in the extracellular model. In the model, proteins are quantified in units of molar concentration, whereas viruses are quantified as discrete numbers of viral particles. Fig. 2 shows the time evolution of total number of A3G(−) and A3G(+) viruses produced in a single cell after infection and released from it to the extracellular environment.

Mathematical Model Development for Extracellular Events ("Multicellular Model")

Our multicellular model describes an extracellular pool of HIV viruses infecting a population of T cells, specifically, in cell culture. This model includes cellular and extracellular properties including the production rate of T cells, rate of infection by HIV viruses, variations in levels of A3G(−) and A3G(+) viruses, and burst size (which is defined as the average number of HIV viruses made by an infected cell). There is a strong link between the intracellular and multicellular models through the burst size and the release distribution of A3G(−) and A3G(+) viruses over time. The multicellular model can be described by a set of equations and constraints. In our model, we define T_0 as the initial number of "Normal" T cells. Each cell lives in the normal state until a HIV virus infects it. "Infected(+)" and "Infected(−)" states correspond
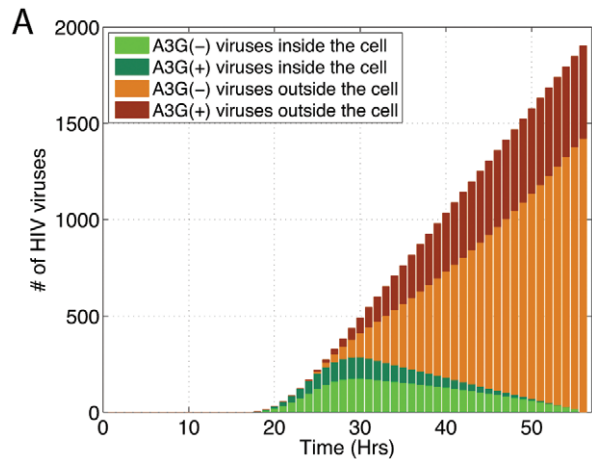

Figure 2. Time-dependent profile of virus release from a single cell. The time evolution of total number of A3G(−) and A3G(+) viruses produced inside a single cell and released from it is shown. Infection occurs at $t = 0$. Production of new viruses begins approximately 16 hours after infection. Light and dark green colors represent A3G(−) and A3G(+) viruses inside the cell. Newly produced viruses get released to the extracellular environment at 22 hours post infection and the virus release continues until the cell dies approximately 55 hours after infection. A3G(−) and A3G(+) viruses outside the cell are represented by light and dark brown colors.
doi:10.1371/journal.pcbi.1002371.g002

to cells that have been infected by A3G(+) and A3G(−) viruses, respectively; however, infected(+) cells produce fewer viruses than infected(−) cells. It is assumed that there is no hyper-infection, that is, after a virus attacks and enters a healthy cell, the cell becomes infected, CD4 is down-regulated [63], and no more viruses attack it. Cells in infected(+) and infected(−) states become "Productive(+)" and "Productive(−)" after $\Delta t = t_{\text{prod}}$ post infection, respectively and begin releasing viruses into the extracellular environment. The release continues until $\Delta t = t_{\text{dead}}$ after infection, when the cell dies and it is marked "Dead". A schematic diagram of cell states is shown in Fig. 3A.

Fig. 3B is a snapshot of the multicellular model at a specific time, showing cells of different post-infection ages at different states. In our simulations, we keep time of infection for each cell in the multicellular model. This is represented by early and late infected cells in the set of infected cells and by early and late productive cells in the set of productive cells.

The number of healthy and infected cells in our model is governed by the following equations.

$$\frac{dT(t)}{dt} = k_p T(t) - k_{inf}(V_{(-)}(t) + V_{(+)}(t))T(t), \qquad (7)$$

and

$$\frac{dT_{\text{inf},(-)}(t)}{dt} = k_{\text{inf}} V_{(-)}(t) T(t) - \\ k_{\text{inf}} V_{(-)}(t - t_{\text{prod}}) T(t - t_{\text{prod}}), \qquad (8a)$$

$$\frac{dT_{\text{inf},(+)}(t)}{dt} = k_{\text{inf}} V_{(+)}(t) T(t) - \\ k_{\text{inf}} V_{(+)}(t - t_{\text{prod}}) T(t - t_{\text{prod}}), \qquad (8b)$$

where T is the number of healthy cells and the rate of infection is defined by k_{inf}. The proliferation rate of healthy cells is represented by $k_p = \ln(2)/t_{T,2}$ where $t_{T,2}$ is the cell doubling time. A3G(−) and A3G(+) viruses are denoted by $V_{(-)}$ and $V_{(+)}$, respectively, and t represents time post inoculation of the T cell culture. Note that $V_{(-)}(t)$, $V_{(+)}(t)$, and $T(t)$ are all zero for t<0. In (7), the number of normal T cells increases by cell proliferation and decreases as cells get infected.

In (8a) and (8b), $T_{\text{inf},(-)}$ and $T_{\text{inf},(+)}$ represent the number of cells infected by A3G(−) and A3G(+) viruses, respectively. As mentioned earlier, each infected cell begins releasing new viruses after a time t_{prod} post infection. At this point, the infected cells become actively productive, represented by $T_{\text{prod},(-)}$ and $T_{\text{prod},(+)}$. Note that in (8a), there are two mathematical terms determining the rate of change for $T_{\text{inf},(-)}$. The first term, $K_{\text{inf}}V_{(-)}(t)T(t)$, represents the number of cells that become infected by A3G(−) viruses at time t and enter the set of infected cells, whereas the second term, $K_{\text{inf}}V_{(-)}(t-t_{\text{prod}})T(t-t_{\text{prod}})$, represents the number of cells that were infected at time $t-t_{\text{prod}}$, i.e., they are productive at time t and leave the set of infected cells to join the set of productive cells (Fig. 3B). The mathematical terms in (8b) are the same as those in (8a), except that they deal with infected(+) cells. The number of productive cells is described by

$$\frac{dT_{\text{prod},(-)}(t)}{dt} = k_{inf} V_{(-)}(t - t_{\text{prod}}) T(t - t_{\text{prod}}) - \\ k_{inf} V_{(-)}(t - t_{\text{dead}}) T(t - t_{\text{dead}}), \qquad (9a)$$
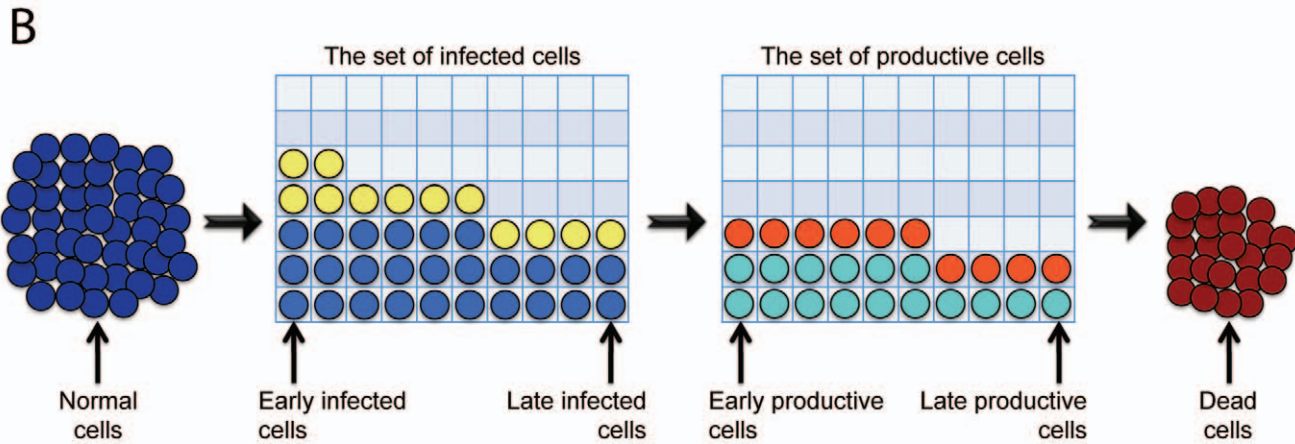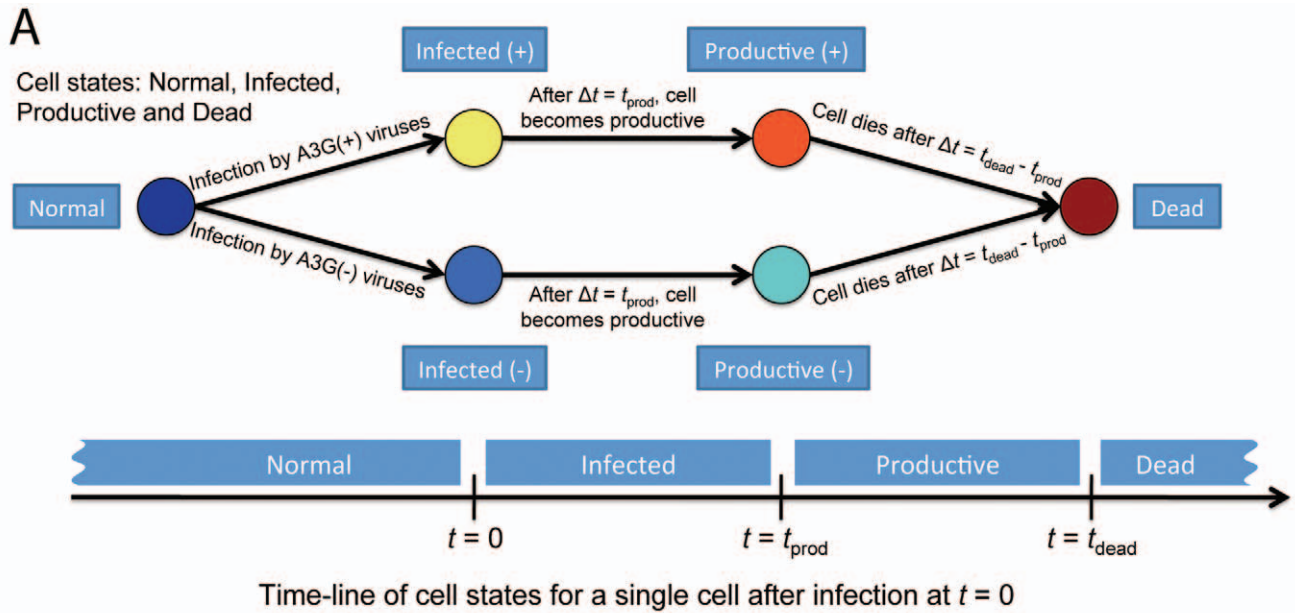
Figure 3. A schematic diagram of cell states and a snapshot of the multicellular model. (A) each cell lives in the "Normal" state until a HIV virus infects it. An "Infected" cell doesn't release new virions until a certain time point post infection, denoted t_{prod}. At this time point, the cell becomes "Productive" and begins releasing viruses into the extracellular environment until it dies at t_{dead}, when it is marked as "Dead". The "Infected(+)" and "Infected(−)" states correspond to cells that have been infected by A3G(+) and A3G(−) viruses, respectively. The same concept applies to "Productive(+)" and "Productive(−)" cells. (B) The time of infection is known for each cell in our multicellular model. A snapshot of the multicellular model shows cells with different post-infection ages in the sets of infected and productive cells. Normal cells become infected and enter the set of infected cells as early-infected cells. The late-infected cells become productive and leave the set of infected cells to join the set of productive cells where they are shown as early-productive cells. Finally, late-productive cells die, exit the set of productive cells, and get marked as dead.

doi:10.1371/journal.pcbi.1002371.g003

$$\frac{dT_{prod,(+)}(t)}{dt} = k_{inf} V_{(+)}(t-t_{prod})T(t-t_{prod}) -$$

$$k_{inf} V_{(+)}(t-t_{dead})T(t-t_{dead}). \tag{9b}$$

In (9a), the first term, $K_{inf}V_{(-)}(t-t_{prod})T(t-t_{prod})$, represents the number of cells that become productive at time t and enter the set of productive cells. Once the cells are infected with HIV, they have an average life span of t_{dead}. This means that productive cells release HIV viruses from t_{prod} until their death at t_{dead}. The second term in (9a), $K_{inf}V_{(-)}(t-t_{dead})T(t-t_{dead})$, represents the number of cells that were infected at time $t-t_{dead}$, i.e., they are dead at time t and leave the set of productive cells (Fig. 3B). The mathematical

terms in (9b) are the same as those in (9a), except that they describe productive(+) cells. The number of dead cells is represented by T_{dead}, governed by

$$\frac{dT_{dead}(t)}{dt} = \frac{dT_{dead,(-)}(t)}{dt} + \frac{dT_{dead,(+)}(t)}{dt}$$

$$= k_{inf} V_{(-)}(t-t_{dead})T(t-t_{dead}) \tag{10}$$

$$+ k_{inf} V_{(+)}(t-t_{dead})T(t-t_{dead}).$$

Along with the equations for different cell states, the model tracks extracellular viruses.

$$\frac{dV_{(-)}(t)}{dt} = pT_{\text{prod},(-)}(t)M_{\text{avg}} + pcT_{\text{prod},(+)}(t)M_{\text{avg}} - \quad (11a)$$
$$k_{\text{inf}}V_{(-)}(t)T(t) - k_v V_{(-)}(t),$$

$$\frac{dV_{(+)}(t)}{dt} = (1-p)T_{\text{prod},(-)}(t)M_{\text{avg}} + \quad (11b)$$
$$(1-p)cT_{\text{prod},(+)}(t)M_{\text{avg}} - k_{\text{inf}}V_{(+)}(t)T(t) - k_v V_{(+)}(t).$$

The average number of viruses released from a productive(−) cell is $M_{\text{avg}} = B/(t_{\text{dead}} - t_{\text{prod}})$ where B is the viral burst size. The percentage of released viruses that do not contain A3G is denoted by p. The encapsulated A3G in the HIV virus has anti-viral activities in the target cell. This results in that a productive(+) cell produces fewer viruses than a productive(−) cell. The reduction in burst size of productive(+) cells is denoted by c. Both p and c take values between 0 and 1. In (11a), the first and second terms refer to the number of A3G(−) viruses being produced from productive(−) and productive(+) cells, whereas the third term represents the number of viruses that are infecting cells. The last term shows the number of viruses that are being cleared from the culture. The clearance rate is represented by $k_v = \ln(2)/t_{v,1/2}$ where $t_{v,1/2}$ is HIV half-life *in vitro*. Mathematically similar terms describe the number of A3G(+) viruses in (11b).

Parameters p and c play important roles in our simulation. Since p has a direct effect on the shape of HIV replication curves (described later), we call this parameter HIV replicative potential. The value of p inversely correlate with intracellular A3G getting encapsulated in newly made viral particles. It is desirable for both p and c to have values as close as possible to zero to efficiently stop HIV replication. Nominal values of p and c are shown in Table 1 for different types of viruses and cells. Note that p is a property of cells whereas c is a property of viruses. To compute the number of A3G(−) and A3G(+) viruses in (11a) and (11b), we assumed that the release rate of viruses from a productive cell over period of $[t_{\text{prod}}, t_{\text{dead}}]$ is constant and also p, the HIV replicative potential remains constant during this period.

As we will see in the results section, the release rate of viruses from a productive cell is not constant at all times. In fact, virus release begins at t_{prod} post infection, increases for 8 hours and remains constant until the cell dies. Also the ratio of released A3G(−) viruses to total released viruses is not constant during the virus release period and changes over time as it can be seen in Fig. 2. Therefore we use the following equations instead of (11a) and (11b) to accurately compute the number of viruses without having any assumptions on the release of viruses.

$$\frac{dV_{(-)}(t)}{dt} = \sum_{i=1}^{T_{\text{prod},(-)}(t)} M_{(-)}(t-t_i) + \quad (12a)$$
$$\sum_{i=1}^{T_{\text{prod},(+)}(t)} cM_{(-)}(t-t_i) - k_{\text{inf}}V_{(-)}(t)T(t) - k_v V_{(-)}(t),$$

$$\frac{dV_{(+)}(t)}{dt} = \sum_{i=1}^{T_{\text{prod},(-)}(t)} M_{(+)}(t-t_i) + \quad (12b)$$
$$\sum_{i=1}^{T_{\text{prod},(+)}(t)} cM_{(+)}(t-t_i) - k_{\text{inf}}V_{(+)}(t)T(t) - k_v V_{(+)}(t),$$

$M_{(-)}(t)$ and $M_{(+)}(t)$ are the number of released A3G(−) and A3G(+) viruses from a single cell at time t after infection, defined in (6a) and (6b). The first term in (12a) is a summation over all the A3G(−) viruses that are being released at time t from all the cells in the set of productive(−) cells. The time of infection for the ith cell in the set is denoted by t_i. The second term in (12a) is similar to the first term, but deals with the A3G(−) viruses released from the productive(+) cells. Similar mathematical expressions are used for computing the number of A3G(+) viruses in (12b).

Viruses in cell culture can become non-infectious or dead after some time. The number of cleared viruses from the culture is given by

$$\frac{dV_{\text{dead}}(t)}{dt} = k_v(V_{(-)}(t) + V_{(+)}(t)). \quad (13)$$

Integration of Single-Cell Model Results into the Multicellular Model

As noted above, the single cell and multicellular models are linked through the burst size and the release distribution of A3G(−) and A3G(+) viruses over time. In this paper, we use the following two methods to establish this link.

In the first method, the multicellular model assumes that release rate of viruses from a productive cell over period of $[t_{\text{prod}}, t_{\text{dead}}]$ is constant and also that the ratio of released A3G(−) viruses to total released viruses at each time point during virus release is constant and equal to p. With these assumptions, $V_{(-)}(t)$ and $V_{(+)}(t)$ can be easily computed using (11a) and (11b). In the second method, the multicellular model makes no assumption on the rate of virus release and uses the actual time-dependent profile of virus release

Table 1. Values of p and c for different cases of viruses and cells.

	A3G(−) viruses	A3G(+) viruses
Target cells express A3G	p = Low, c≈1	p = Low, c≈Low
	Output: A3G(−) and A3G(+) viruses	Output: A3G(−) and A3G(+) viruses
Target cells do not express A3G	p≈1, c≈1	p≈1, c≈Low
	Output: only A3G(−) viruses	Output: only A3G(−) viruses

from a single cell to compute the total number of A3G(−) and A3G(+) viruses in culture supernatant by using (12a) and (12b). Although this method provides a comprehensive link between the two models, it would be difficult to optimize the system parameters. Therefore, we use the first method for optimizing the single-cell and multicellular model parameters. Having done that, we use the second method for our simulations regarding effects of A3G-based therapeutic strategies, drug penetrance and administration time on HIV replication.

Results

Single-Cell Model of APOBEC3G-Vif Interactions

For our simulations, we obtained parameters from published biological experiments. Several groups have measured the degradation profiles of Vif and of A3G in the presence and absence of Vif [38,41,64,65]. First-order kinetic decay curves were used to approximate the degradation rate of Vif, A3G, and A3G-Vif complex from this experimental data as 0.25 hr^{-1}, 0.1 hr^{-1}, and 0.3 hr^{-1}, respectively (Figs. 4A–C). The binding affinity of A3G to Vif has been estimated to be in the low micromolar range by surface plasmon resonance [66]. We assume a value of 1 µM for the binding affinity, and calculate k_{on} by assuming $k_{off} = 3600$ hr^{-1}. The stoichiometry of A3G and HIV, i.e., the number of A3G proteins incorporated into a virion, s_{A3G}, has been estimated at seven molecules [67]. In an infected cell, viral protein production does not start as soon as HIV enters in the cell. Based on published experimental studies, Vif production begins approximately 12 hours after infection ($t_{prod,Vif} = 12$ hr), increases through 24 hours ($\Delta t_{rise,Vif} = 12$ hr) and remains roughly constant after that. This was experimentally observed by measuring expression of HIV-1 RNA transcripts during HIV infection in [68,69] and computationally verified in [57]. HIV particle formation is assumed to begin 16 hours post infection ($t_{form,HIV} = 16$ hr), continue to increase for 8 hours ($\Delta t_{rise,HIV form} = 8$ hr) and plateau after that. In addition, a 6-hour delay is assumed for the budding process, meaning that virus release begins at 22 ($t_{rel,HIV} = 22$ hr) and increases through 30 hours post infection ($\Delta t_{rise,HIV rel} = 8$ hr). These assumptions are consistent with measurements of reverse transcriptase activity in cell culture supernatants indicating active release of viruses from cells [69] and with the predictions of theoretical modeling [57].

Using the above parameters as a basis, we estimated the production rates of A3G and Vif. We have not found experimental data quantifying these production rates, therefore, we estimate these parameters using data from [11]. In those experiments, 293T cells were used as a 'permissive' cell line, meaning that they did not express A3G intrinsically. These cells were co-transfected with two vectors: one either a wild-type (WT) or a Vif-deficient (ΔVif) X4 provirus; the other (at varying doses) encoding A3G. After a day, the levels of supernatant p24 protein in the culture were monitored. The number of viruses can be calculated from this, as the 24-kDa p24 protein is estimated to be present at 2000–4000 molecule per virion [70], therefore 1 pg p24≈12,500 HIV particles. The supernatant including viruses from the infected 293T cells was extracted, normalized by p24 content, and used to challenge indicator cell lines in a single-cycle infection assay in which expression of chloramphenicol acetyltransferase (CAT) indicated HIV infection. After 28 hours, the number of infected cells were measured and normalized [11]. We use the single-cell model to find the percentage of released A3G(−) viruses in culture in the transfection part of this experiment and employ the multicellular model with equations (11a) and (11b) for the inoculation of CAT-indicator cells. Although the first part of this
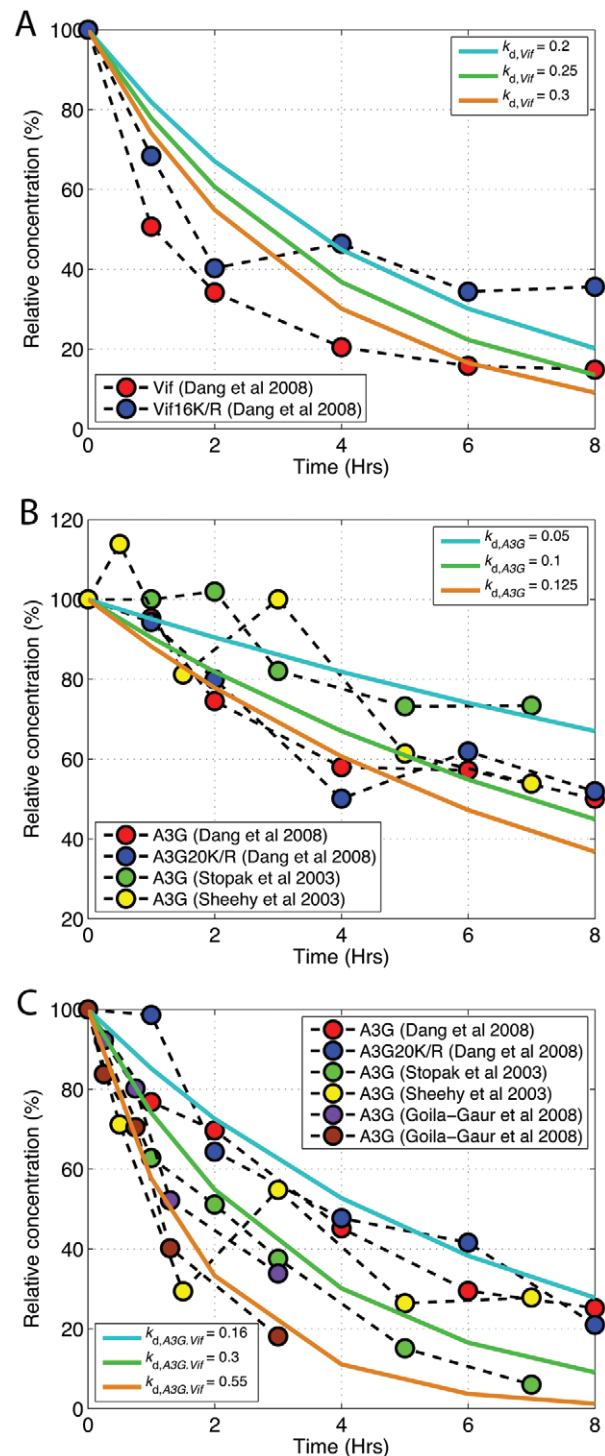

Figure 4. Degradation profile of protein entities in the model. Using experimental data and first-order decay curves, degradation coefficients of (A) Vif, (B) A3G, and (C) A3G-Vif complex were estimated to be 0.25 hr^{-1}, 0.1 hr^{-1}, and 0.3 hr^{-1}, respectively (re-plotted from Benedict et al. [60]).
doi:10.1371/journal.pcbi.1002371.g004

algorithm is a transfection of a T cell culture, information on the number of cells and transfection efficiency was not available. Moreover, we know that cells begin releasing viruses 22 hours after infection and in this experiment the culture supernatant was extracted 24 hours after transfection. This means that viruses in

the supernatant were released from cells that were infected in the first two hours after transfection. Therefore, asynchronous infection would not be an issue in this case. This justifies using the single-cell model for the transfection part of this experiment.

Estimation of Vif and A3G production rates required an exhaustive search in P_{Vif}-P_{A3G} domain. The procedure is as follows. For a given pair of (P_{Vif}, P_{A3G}), the single-cell model computes the HIV replicative potential, the percentage of released viruses that are A3G(−). Next, in the multicellular model, CAT-indicator cells ($T_0 = 500,000$ cells) are inoculated by viruses corresponding to 5 ng p24 with the ratio of A3G(−) to total viruses equal to p. The simulations are run for three different doses of A3G as in the experiment: (P_{Vif}, P_{A3G}), (P_{Vif}, $P_{A3G}/3$), and (P_{Vif}, $P_{A3G}/6$), and the number of infected cells at 28 hours is computed, normalized and compared to the experimental results to calculate the fitness error which is defined as the square root of sum of squares of differences between experimental data and computed results. For the HIV-ΔVif case ($P_{Vif} = 0$ μM/hr), the error for a range of P_{A3G} is depicted in Fig. 5A and the minimum error is achieved at $P_{A3G} = 0.085$ μM/hr.

In contrast, Fig. 5B shows the error for the HIV-WT case for a wide range of values of P_{Vif} and P_{A3G}. The fitness increases from low to high as the color changes from red to dark blue. This figure gives us possible pairs of (P_{Vif}, P_{A3G}) producing best fits to the experimental data. Based on the value of P_{A3G} obtained from Fig. 5A, the best fit is achieved at $P_{Vif} = 33$ μM/hr. The experimental data from Sheehy et al. [11] used for calculating P_{Vif} and P_{A3G} is re-plotted as blue bars in Figs. 5C and 5D for WT and ΔVif viruses, respectively. The red bars show model predictions of percentage of CAT cells infected by using optimized P_{A3G} and P_{Vif} in our simulations.

The estimates of P_{A3G} and P_{Vif} were computed for an assumed value of $k_{A3G.HIV} = 50$ μM^{-1}/hr, because A3G incorporation rate is not known. We repeated the simulations for a range of $k_{A3G.HIV}$ values and estimated values of P_{A3G} and P_{Vif} with the minimum error are shown in Fig. 5E and Fig. 5F. We found that P_{A3G} is inversely proportional with $k_{A3G.HIV}$, whereas P_{Vif} remains approximately constant. For the rest of this paper, we use the average value of P_{Vif}, which is equal to 35.6 μM/hr. For the estimation of P_{Vif} and P_{A3G}, optimal values for burst size, infectivity rate and HIV half-life in vitro were used in the multicellular model. These parameters will be discussed in the next section.

Multicellular Model of HIV Propagation in Culture

For the HIV replication experiments that we are simulating in this section, unlike the single-round infectivity experiments above, there is sufficient time for new viruses released by the cells to infect other cells. In these simulations, we assume that permissive or non-A3G expressing CEM-SS cells are used, with $t_{T,2} = 30$ hours ($k_p = 0.5545$ day^{-1}) [71,72]. In the multicellular model, we focus on the release of new HIV. This begins approximately 0.9 days post infection [53,57,69], so $t_{prod} = 22$ hours. Also, on average a life-span of 2.3 days was estimated for infected cells [53], therefore $t_{dead} = 55$ hours. In exploring the multicellular model, we assume that the release rate of viruses is constant during the productive phase. Later, when we integrate the single-cell model, the actual time-varying distribution of virus release is employed. Several estimates using different techniques are available, ranging from a hundred to a few thousand viruses per cell [73–79]. HIV clearance rate in vivo has been estimated in the range of a few hours to a couple of days [53,80–82], however, measurements of HIV clearance rate in vitro are not available. Using experimental data in [11], we estimate k_{inf}, B, and $t_{v,1/2}$. In [11], CEM-SS cells ($T_0 = 500,000$) were stably co-transfected with either an A3G- or

neo-encoding vector. Then, both cell lines were inoculated by either ΔVif or WT viruses with an initial dose of 1 or 10 ng p24. Accumulation of p24 in the culture supernatants was monitored over time. As expected, efficient replication of both WT and ΔVif viruses was observed in the neo-expressing cells. The A3G-expressing cells also supported WT virus growth, however, very low replication of ΔVif viruses was observed.

Since WT HIV replication in both neo- and A3G-expressing cells were almost the same, we conclude that the amount of A3G was insufficient to have a large effect on WT HIV replication, suggesting that Vif had completely inhibited A3G and most of newly produced viruses did not contain A3G. Therefore, even though we have A3G-expressing cells, we assume $p = 1$. Hereafter, we dismiss neo-expressing cells and only focus on A3G-expressing cells. Data points taken from the published experiments describing the increase in WT HIV numbers in vitro are shown in Fig. 6A with red and blue squares representing 1 and 10 ng p24 input HIV, respectively. As seen in Fig. 6A, data points corresponding to 1 ng p24 start at 0.1 ng p24/ml on day 3 after inoculation of cell culture. This means that the volume of cell culture was equal to 10 ml. In our simulations, the blue data points (10 ng p24) are used as training data for parameter estimation. Then, we change the initial dose to 1 ng p24 while keeping the estimated parameters fixed and run the model to examine how well it can reproduce the red data points.

Given a specific value for viral half-life $t_{v,1/2}$, we used the default nonlinear curve-fitting function in Matlab to find the optimum pair of burst size and infectivity (B, k_{inf}) such that the simulated HIV growth curve fits the experimental data (WT - 10 ng p24) with the minimum fitness error. This error is the discrepancy between experimental and computational results defined by square root of sum of squares of differences between experimental data and computed results at each observation time point. We studied the effects of HIV half-life and cell doubling time on these estimates of optimal B and k_{inf} in Fig. 7A and Fig. 7B. As $t_{v,1/2}$ increases, the estimated value of k_{inf} decreases while estimated burst size stays roughly the same. However, as $t_{T,2}$ changes from 18 to 48 hours, the estimates of B increase approximately from 400 to 5900 while the values of k_{inf} decrease less than an order of magnitude. This is reasonable in a sense that in order to get the same amounts of HIV output as $t_{T,2}$ increases, viruses must infect with lower rates ($k_{inf} \downarrow$), however, they must produce more progeny in the cells ($B \uparrow$). Since we know $t_{T,2} = 30$ hours, only the optimum values of B and k_{inf} for each value of $t_{v,1/2}$ are shown in Table 2.

For each set of parameters in Table 2, simulated HIV growth curves are shown in Fig. 6A with dark blue representing $t_{v,1/2} = 24$ hours and light blue representing other values for $t_{v,1/2}$ in the range of 4 hours to infinity. The curves overlap and are a good fit for the blue squares. HIV growth curves with the same parameters and 1 ng p24 HIV input are also depicted in Fig. 6A with dark ($t_{v,1/2} = 24$) and light ($t_{v,1/2} = 4 \ldots$ Inf) red colors. Again, it is observed that all the curves are similar and provide a good fit for the red data points, with the exception of the last square, which we will discuss later. Therefore, none of the tested values for viral half-life, $t_{v,1/2}$, can be dismissed at this point, since all of them have generated good fits for the experimental data.

Now, we focus on the experimental data obtained from 10 ng p24 ΔVif viruses (blue circles in Fig. 6B). HIV growth curves corresponding to different values of $t_{v,1/2}$ increasing from the lowest curve to the highest one are also shown in Fig. 6B. These curves were generated as follows. For each triplet of values for ($t_{v,1/2}$, B, k_{inf}) from Table 2, the optimal values of p and c between 0 and 1 were chosen using Matlab's built-in nonlinear curve-fitting function
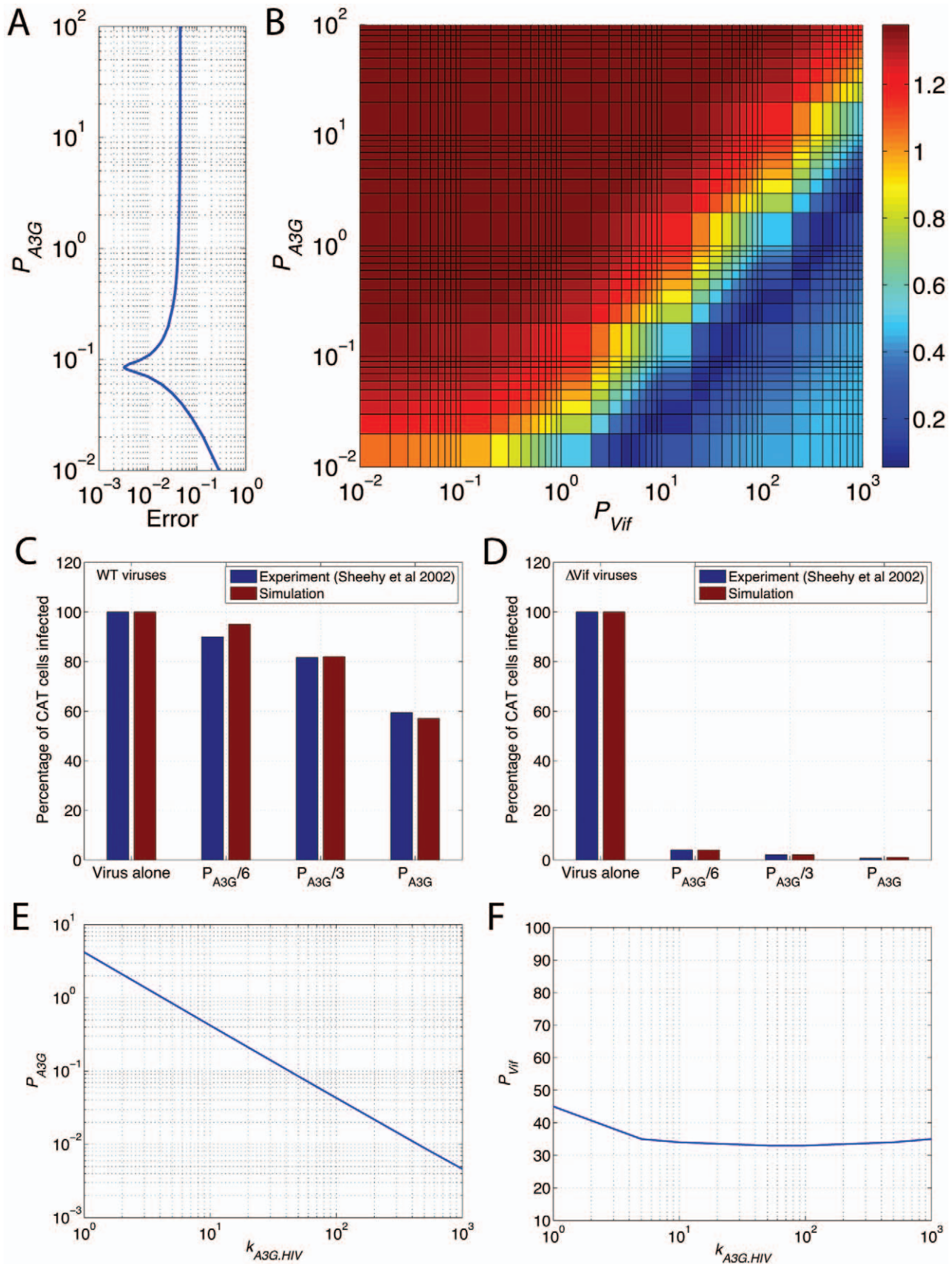
Figure 5. Estimation of A3G and Vif production rates. (A) shows the optimum P_{A3G} for the ΔVif case ($P_{Vif} = 0$), whereas (B) shows the fitness error heat-map for a wide range of values of (P_{Vif}, P_{A3G}) for the WT case. The error decreases as color changes from dark red to dark blue. The optimum P_{A3G} can be read from (A) and projected to the dark blue region of (B) to find the optimum P_{Vif}. The experimental data from Sheehy et al. [11] were

used for estimating P_{Vif} and P_{A3G} is re-plotted as blue bars for (C) WT and (D) ΔVif viruses. The red bars show our predictions of percentage of CAT cells infected by using estimated P_{A3G} and P_{Vif} in our simulations. All the results in (A) and (B) are obtained for $k_{A3G.HIV} = 50 \ \mu M^{-1}$/hr. The optimum values of (E) P_{Vif} and (F) P_{A3G} versus $k_{A3G.HIV}$ are also shown.
doi:10.1371/journal.pcbi.1002371.g005

such that the generated curve provided the lowest error (deviation from experimental data). Although all the values of $t_{v,1/2}$ could provide a good fit to the experimental data points in Fig. 6A, they all failed to produce good fits to the blue circles in Fig. 6B except $t_{v,1/2} = 24$ which provided a good match with $p = 0.008$ and $c = 0.008$. Therefore, we conclude that HIV half-life *in vitro* is approximately 24 hours and we use this number and corresponding numbers from Table 2 for burst size and infectivity rate in the rest of this study. Note that these are the optimal values of $t_{v,1/2}$, B, and k_{inf} that were used in multicellular model in the last section where we estimated P_{Vif} and P_{A3G}.

In Fig. 6C, red circles correspond to 1 ng p24 ΔVif input and a simulation curve using the estimated parameters is superimposed. This curve is a reasonable fit to the data points except for the last red circle. Compared to the 10 ng p24 data, the experimental data points for 1 ng p24 ΔVif input are noisy, possibly because of the small amounts of p24 in culture supernatant which are initially close to the detectable level of the p24 ELISA assay.

At this point, we must ask: why do the simulated HIV growth curves saturate around 9–10 days after infection in the case of WT viruses? In order to explain this, we study the distribution of cell states during the period of post infection. As seen in Fig. 8A for the
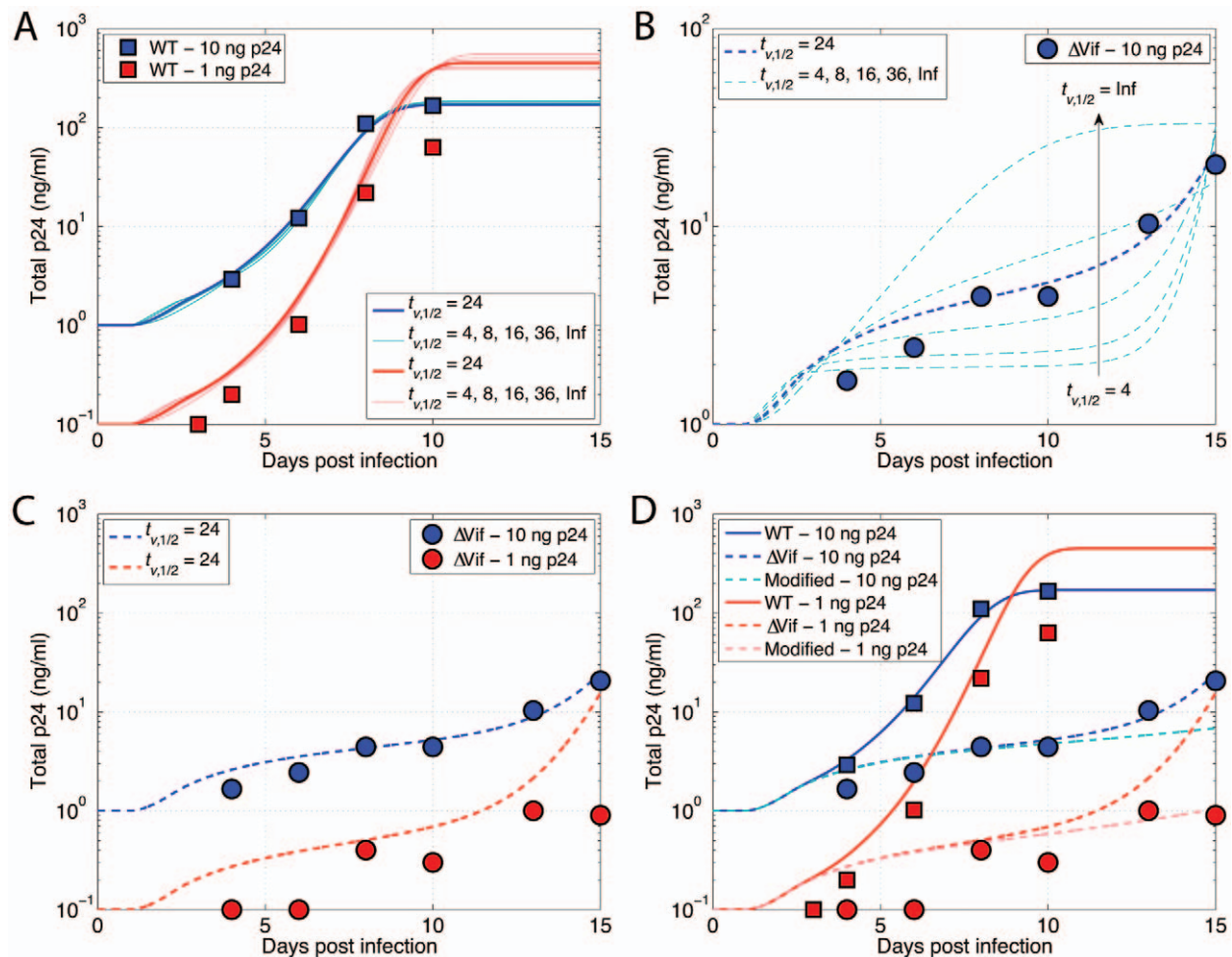

Figure 6. HIV growth curves for WT and ΔVif viruses. (A) Inoculation of cultures of 500,000 cells with WT HIV. Blue and red squares represent 1 and 10 ng p24 HIV input, respectively. For a given $t_{v,1/2}$, values of burst size and virus infectivity rate were estimated such that the resulting simulated HIV growth curve fitted the blue data point with the minimum fitness error (shown as blue lines for $t_{v,1/2} = 4, 8, 16, 24, 26,$ Inf hours). Then, the estimated numbers were used to predict experimental data points corresponding to 1 ng p24 (shown as red lines). (B) Inoculation by 10 ng p24 ΔVif HIV. For each triplet of ($t_{v,1/2}$, B, k_{inf}) from (A), the values of p and c between 0 and 1 were chosen such that the generated curve provided the smallest error. None of the values of $t_{v,1/2}$ produced good fits to the blue circles except $t_{v,1/2} = 24$ hours where p and c were estimated to be 0.008 and 0.008, respectively. (C) The estimated parameters for $t_{v,1/2} = 24$ hours from (A) and (B) were used to examine how well they could generate a curve to fit experimental data points corresponding to 1 ng p24 ΔVif input (red circles). The red dashed line provided an acceptable fit to the data points except for the last circle where the line diverged. (D) All the experimental data points as well as their HIV growth curves are shown in red and blue colors corresponding to 1 and 10 ng p24 HIV input. Also, we included crowding effects in our simulation by using a logistic function. The two new curves drawn in light red (1 ng p24 ΔVif) and light blue (10 ng p24 ΔVif) show the HIV growth curves for this case. It can be seen that these curves provide a better fit to the experimental data than the curves in (C).
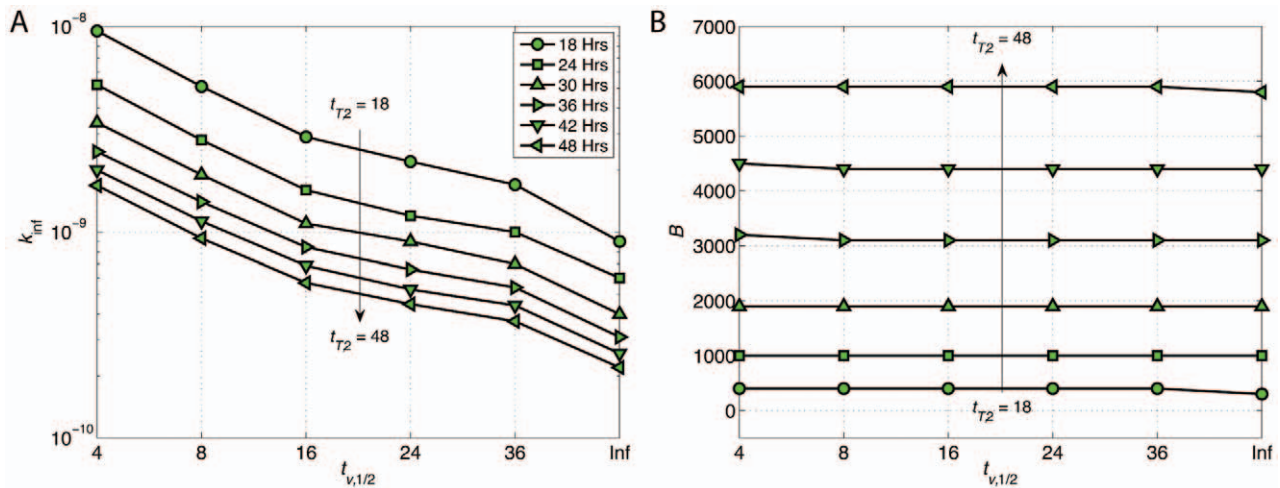doi:10.1371/journal.pcbi.1002371.g006

Figure 7. Effects of HIV half-life and cell doubling time on virus infectivity rate and burst size. (A) k_{inf} decreases as $t_{T,2}$ changes from 18 to 48 hours. The same trend is also observed as $t_{v,1/2}$ increases from 4 hours to infinity. (B) Estimated burst size remains almost the same for different values of $t_{v,1/2}$, however, it increases as $t_{T,2}$ goes up.
doi:10.1371/journal.pcbi.1002371.g007

case of 10 ng p24 WT HIV input, normal cells dominate from the beginning of infection until the 8th day. But as infection progresses, infected cells begin to take over. These cells begin production of new viruses at around 22 hours after infection so the dominant cells on the 9th day are productive cells. Finally, viruses kill the productive cells at around 55 hours post infection and thus after the 11th day, almost all the cells in the culture are dead. Therefore, no more viruses can be produced and the HIV growth curve plateaus. The same scenario is observed in Fig. 8B (WT – 1 ng p24), however, infection progresses more slowly due to presence of fewer viruses initially. As seen in Fig. 8B, the number of normal cells is much higher than the previous case in the period of days 1–9. This explains why the total number of viruses will eventually be higher than the case of 10 ng p24 WT in Fig. 6A. The reason is that many more normal cells are available for HIV infection in the case of 1 ng p24 WT, which results in production of more viruses in the model. This is a testable prediction of the model, which would require the experiment to be continued after 10 days.

Looking at Fig. 8D for ΔVif viruses, we see more than 80 percent of the cells are healthy on the 15th day and the percentage of dead cells is negligible, in clear contrast to what was seen for WT viruses in Figs. 8A–B. This is because of the less efficient propagation of infection of ΔVif viruses allowing normal proliferation of healthy cells. This in turn provides yet more cells

for HIV to infect compared to the WT case. In fact, it may explain the rise of the ΔVif growth curve in Fig. 6C and its divergence from the experimental data points. In our model, we have assumed constant cell proliferation rates, however, cells might slow or even stop proliferation when the suspension becomes crowded. In order to test whether this was a possible explanation for the observed data, we included the crowding effects in our model by using the logistic function. Therefore, (7) is replaced by

$$\frac{dT(t)}{dt} = k_p T(t)\left(1 - \frac{T(t)}{T_{max}}\right) - k_{inf}(V_{(-)}(t) + V_{(+)}(t))T(t), \quad (14)$$

where T_{max} is the maximum possible number of normal cells in culture and we set it to 50,000,000 (5,000,000 cells/ml). Modified ΔVif growth curves are shown in Fig. 6D with light blue and red colors for 10 and 1 ng p24 ΔVif input, respectively. These curves show better fits to the experimental data, suggesting that crowding effects and slow proliferation could explain the experimental results. The distributions of cells states corresponding to these two cases are shown in Figs. 8E–F.

Effects of A3G-Based Therapeutic Strategies, Drug Penetrance and Administration Time on HIV Replication

Using the model parameterized as above, we can compare the predicted efficacy of several therapeutic approaches targeting Vif-A3G interactions. Here, we add four specific molecules to the model and simulate the effect of their intracellular expression. All four are large proteins, as opposed to small molecules, and expression would in most cases require gene therapy. However, small molecules that had similar properties or effects on the functional A3G-Vif network could be delivered orally or intravenously [83,84]. The molecules are: **Ab-Vif**, a high-affinity antibody to Vif [85]; **A3G**, APOBEC3G itself, which could be upregulated by cytokines such as IL-2 [86] or NFAT and IRF proteins [87]; **A3G$^{\Delta Ub}$**, a mutated A3G with lower Vif-induced degradation rate (e.g., C97A-A3G [88]); and **A3G$^{\Delta Vif}$**, a mutated A3G that does not bind Vif (e.g. A3G/F126-129 [89] and D128K-A3G [90]).

In the single-cell model, Ab-Vif is modeled as a new protein with an affinity for Vif 100 times that of A3G. The degradation

Table 2. Estimations of burst size and virus infectivity rate for $t_{T,2} = 30$ hours.

$t_{v,1/2}$ (hr)	B	k_{inf} (day^{-1})
4	1900	34×10^{-10}
8	1900	19×10^{-10}
16	1900	11×10^{-10}
24	1900	9×10^{-10}
36	1900	7×10^{-10}
Inf	1900	4×10^{-10}

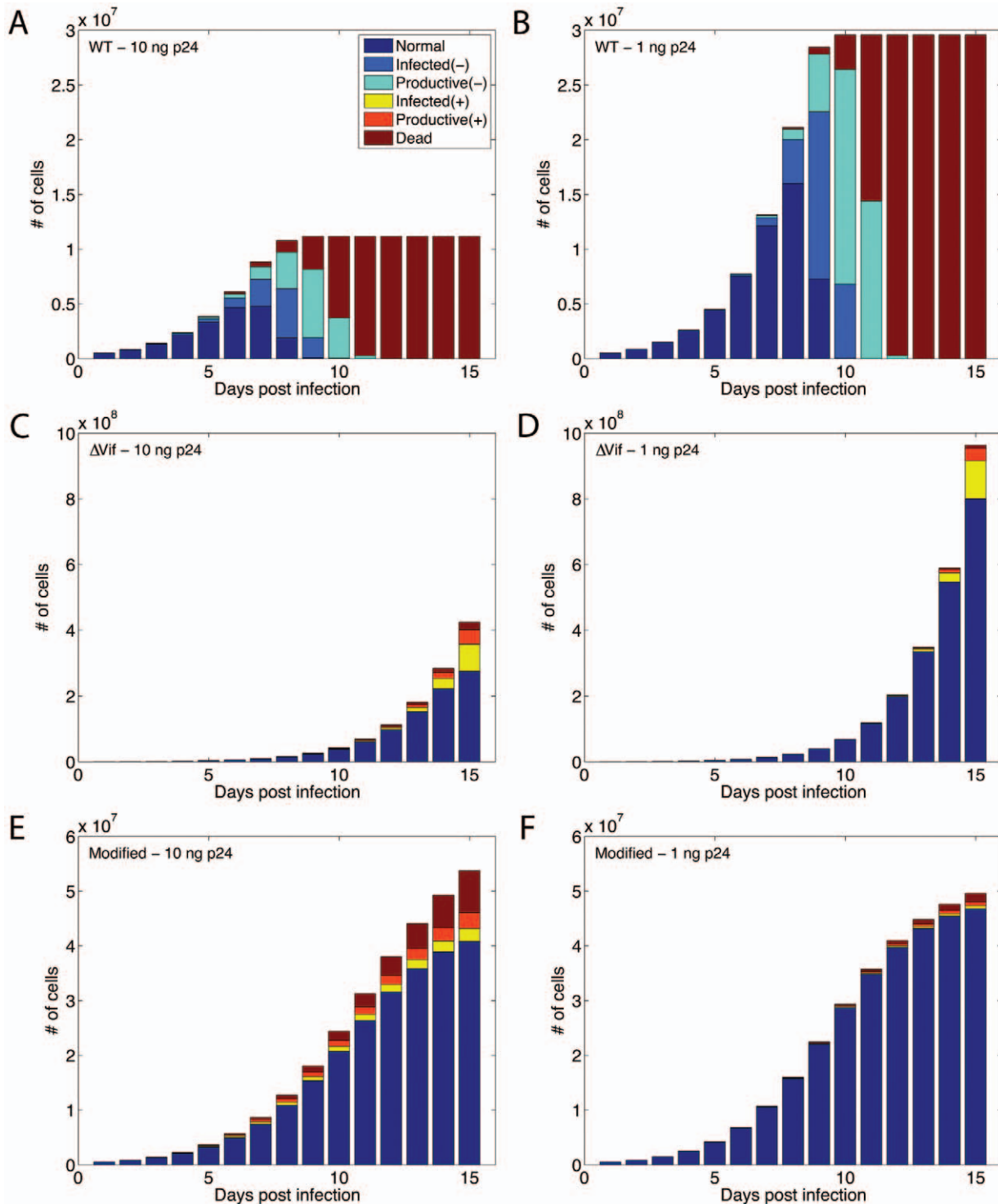doi:10.1371/journal.pcbi.1002371.t002

Figure 8. Distribution of cell states during the period of post infection. We simulated cultures of 500,000 healthy normal cells inoculated by either (A) 10 ng p24 or (B) 1 ng p24 WT HIV input. The infected cells start producing new virions after 22 hours and eventually die around 55 hours after infection. For WT HIV input, most of the cells are dead by the 12th day. In contrast, if we inoculate the cultures with either (C) 10 ng p24 or (D) 1 ng p24 ΔVif viruses, the healthy cells will still be the majority ones and the number of dead cells is negligible on the 15th day. In a different scenario, we included effects of cell culture crowding in our multicellular model by using a logistic function. Such cultures inoculated with either (E) 10 ng p24 or (F) 1 ng p24 ΔVif viruses provide better fits to biological experiments.
doi:10.1371/journal.pcbi.1002371.g008

rate of the complex formed by antibody bound to Vif is assumed to be $k_{d,Vif}$. Upregulation of A3G is modeled by increasing P_{A3G}. A3G$^{\Delta Ub}$ is a mutated A3G that binds to Vif, but its complex with

Vif is not degraded faster than unbound A3G. Therefore, the degradation rate of A3G$^{\Delta Ub}$-Vif complex is assumed to be $k_{d,A3G}$. Finally, A3G$^{\Delta Vif}$ has the binding site for Vif mutated, and so does

not bind to Vif. Note that we also assumed that each of these therapeutic proteins has the same degradation rate as of A3G. In our simulations, each of the drugs is expressed *in addition* to the cellular A3G produced (at a rate of P_{A3G}). The efficacy of each drug in terms of reduction in HIV replicative potential versus various production rates is shown in Fig. 9 for $k_{A3G.HIV} = 5$, 50 and 500 μM^{-1}/hr. Among the therapeutic approaches, Ab-Vif shows a very poor performance even at very high production rates. It should be noted that Ab-Vif on its own can only block Vif from binding to A3G; in other words, it can make A3G more available but cannot add to its function. At least some A3G must be present in the cells to get incorporated into HIV particles. This explains the characteristic plateau as Ab-Vif expression increases (Fig. 9); beyond this point all A3G is available to be encapsulated. A3G and A3G$^{\Delta Ub}$ have efficacy profiles that are similar to each other, both better than that of Ab-Vif. That A3G$^{\Delta Ub}$ is predicted to work only slightly better than A3G suggests that Vif-induced degradation of A3G through proteasomal pathway is not central to Vif effectiveness. A3G$^{\Delta Vif}$ is predicted to be the best therapeutic approach among these drugs, two orders of magnitude better than A3G and A3G$^{\Delta Ub}$. This further suggests that the binding of A3G to Vif is an important interaction that should be inhibited to block HIV replication.

We next study A3G$^{\Delta Vif}$ in the multicellular model, assuming 1 ng p24 WT input and $k_{A3G.HIV} = 50$ μM^{-1}/hr, although qualitatively similar results will be obtained for other values of HIV inputs and $k_{A3G.HIV}$ (data not shown). The intracellular and multicellular models were coupled using (12a) and (12b) to compute the total number of A3G(−) and A3G(+) viruses in culture supernatant. Figs. 10A–D show HIV growth curves corresponding to various production rates of A3G$^{\Delta Vif}$. The blue and red lines represent A3G(−) and A3G(+) viruses, respectively, whereas, the greens lines represent total viruses in culture supernatant including A3G(−), A3G(+), and dead ones. As seen in Fig. 10D, for $P_{A3G\Delta Vif} = 10^2$, HIV replication slows more than two orders of magnitude and A3G(−) viruses reach a level of 10^{-4} by the 10th day. However, A3G(+) viruses start boosting by the 12th day. As mentioned earlier, this is caused due to an unconstrained proliferation of normal cells that provides a huge number of susceptible cells for infection. Similar to before, we constrained proliferation by including crowding effects using a logistic function (dashed lines in Fig. 10). In this case, A3G(+)

viruses reach a stable level below 10^{-1} ng p24/ml and decrease very slowly up to the 15th day. Therefore, A3G$^{\Delta Vif}$ has actually been able to stop HIV replication. A comparison of model predictions using equations (11a/b) or (12a/b) as the coupling method is shown in Supplemental Fig. S1.

At this point, we are interested to study the effects of drug penetrance on HIV replication when only a specific fraction of cells have been transfected ($P_{A3G\Delta Vif} = 10^2$). Figs. 10E–H show HIV growth curves with penetrance = 10, 90, 95 and 100% of cells. It is observed that even if the drug is available to 95% of the cells, viruses can still actively replicate until they kill all the cells in the solution. This suggests that the drug must be available to almost 100% of the cells in order to be effective. HIV growth curves with similar penetrances for the constrained proliferation case are also depicted in Figs. 10E–H. Even in this case, there is a large gap between curves corresponding to 95 and 100% drug availability.

In the next set of simulations, we studied the effects of drug administration time on the virus replication ($P_{A3G\Delta Vif} = 10^2$, penetrance = 100%). As seen in Fig. 10K, if the drug is administered on the 9th day, the HIV growth curve is almost similar to the case that no drug was available to the cells at all as shown in Fig. 10L. Note that these results were obtained for *in vitro* cases, where a constant source of cell production is not available as opposed to *in vivo* cases where old cells proliferate and new cells are born. Also, it should be mentioned that more than 50% of the cells are either infected or productive on the 9th day (Fig. 8B) and a lot of viruses are available in culture supernatant. Therefore, administration of drug to remaining cells cannot help the culture survive. However, cells in the culture can still survive if we administer the drug before the 7th day. This suggests that the drug must be available to the cells shortly after inoculation in order for the drugs to be effective. *In vivo*, the situation would be different; the constant birth of new cells may give this therapy greater hope of success.

Sensitivity Analysis: Determining Critical Model Parameters that Influence HIV Replication

In this section, we analyze the effects of parameter variations in both single-cell and multicellular models. For the intracellular model, we investigate the deviations of HIV replicative potential resulted from +5% change in each of the 17 model parameters (Fig. 11A). As seen, $t_{form,HIV}$, the particle formation starting time,
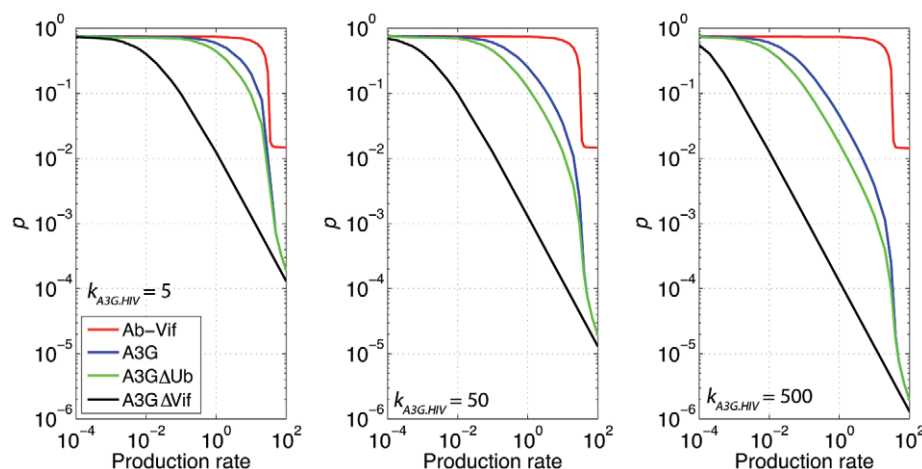

Figure 9. Efficacy comparison of several drugs for different production rates. Efficacy of several proposed therapeutic proteins in reducing the parameter p estimated using the single-cell model for (A) $k_{A3G.HIV} = 5$, (B) 50 and (C) 500 μM^{-1}/hr. For all cases, A3G$^{\Delta Vif}$ shows a better performance than other drugs.
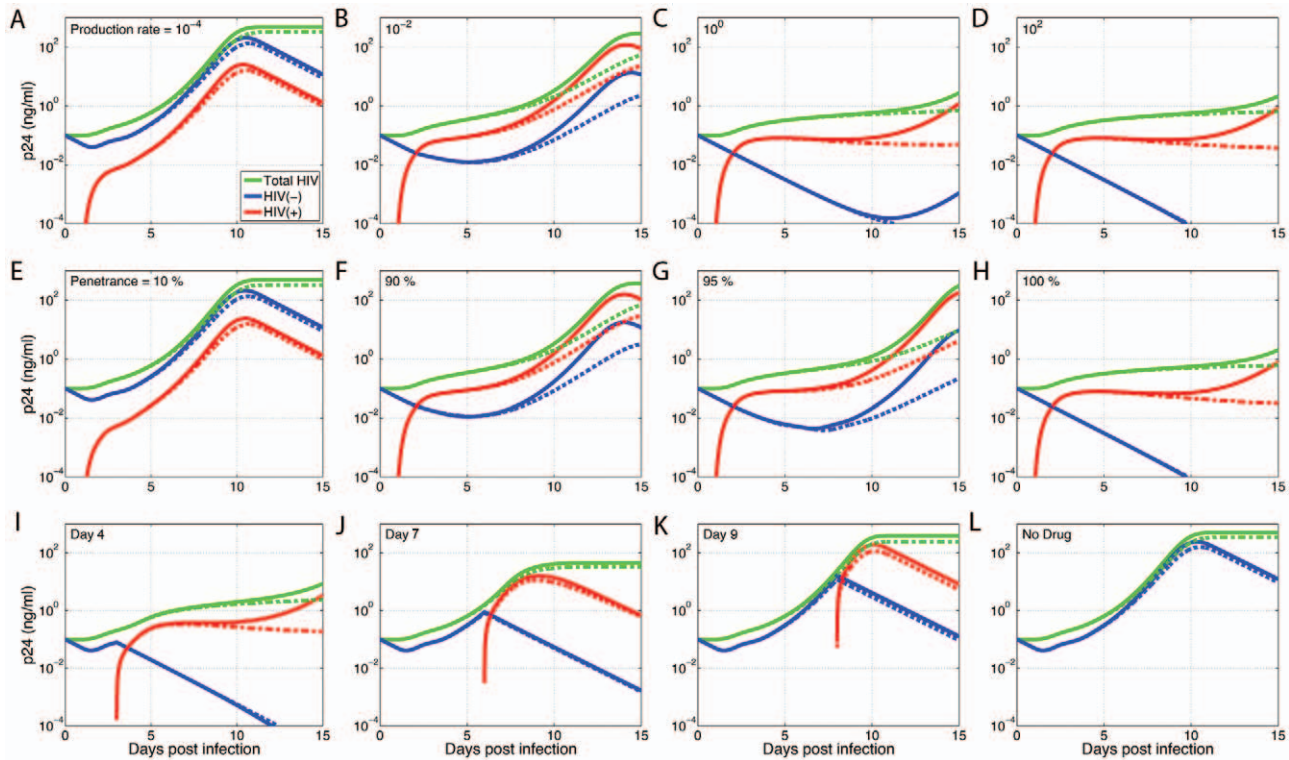doi:10.1371/journal.pcbi.1002371.g009

Figure 10. Effects of different production rates, penetrances and administration times of A3G$^{\Delta Vif}$ on HIV growth curve. In all the simulations, 500,000 cells were inoculated by 1 ng 24 WT HIV input. (A–D) A3G$^{\Delta Vif}$ with different production rates were administered right after inoculation. The red and blue lines represent A3G(−) and A3G(+) viruses in the culture, respectively. The green lines characterize all the viruses including A3G(−), A3G(+), and dead ones. For $P_{A3G\Delta Vif} = 10^2$, the amount of A3G(−) viruses decay to 10^{-4} ng p24/ml by the 10th day, however, the number of A3G(+) viruses rises on the 12th day. Dashed lines represent cultures with constrained proliferation (crowding effects modeled by using a logistic function). In this case, it is seen that A3G(+) viruses reach a stable level below 10^{-1} ng p24/ml and decrease very slowly up to the 15th day for $P_{A3G\Delta Vif} = 10^2$. This suggests that A3G$^{\Delta Vif}$ has been able to stop HIV replication. (E–H) Effects of drug penetrance on HIV growth curves. We simulated cases where the drug was only available to a fraction of cells ($P_{A3G\Delta Vif} = 10^2$). Comparing cases corresponding to 95% and 100%, we can see that there is a gap larger than two orders of magnitude between the total levels of p24 on the 15th day. This implies that drugs should be available to all the cells to get the desired efficacy. The same qualitative effect is observed in the cultures with constrained proliferation for different drug penetrances. (I–L) Effects of administration time on HIV growth curves ($P_{A3G\Delta Vif} = 10^2$ and penetrance = 100%). It is seen that administering drug on the 9th day is not effective and the results are similar to the case of no drug. However, if the drug is administered before the 7th day, cell could still survive. The same trend in effects of drug administration time is also observed in cultures with constrained proliferation.
doi:10.1371/journal.pcbi.1002371.g010

had the highest positive impact on p, whereas $t_{\rm rel,HIV}$, the virus release starting time, had the highest negative impact. This suggests that if the assembly and budding process of HIV particles from the cells could somehow be slowed, it would have a significant effect on virus replication. On the other hand, some of the parameters such as s_{A3G}, burst size, and $k_{\rm d,A3G}$ had very negligible effects on the intracellular model output.

For the extracellular model, two outputs are considered for sensitivity analysis; 1) number of healthy cells and 2) number of A3G(−) viruses on the 6th day. In our simulations, 1 ng p24 WT HIV input was used for infection without administering any drug. In terms of the 1st output, almost none of the parameters had a major impact except the proliferation rate, k_p, which produced high variations in the number of normal cells (Fig. 11B). In contrast, all the multicellular parameters had significant effects on the levels of A3G(−) viruses (Fig. 11C). Considering the combined effects on both outputs, k_p was detected as the most sensitive parameter in the multicellular model.

Discussion

We have developed a mathematical model of the HIV lifecycle inside and outside of cells, using differential equations. Our model is the first one developed to specifically couple molecular-level events within individual cells to the viral dynamics and multiple cycles of infection within a population of cells. In this paper, we used two different methods to couple the two models. Estimation of the system parameters was done using the model with equations (11a) and (11b) in which the release rate of viruses was assumed to be constant over period of $[t_{\rm prod}, t_{\rm dead}]$ and also p remained constant during this period. For the rest of our simulations to study effects of A3G-based therapies, the model with equations (12a) and (12b) was used in which the time-dependent distribution of virus release from a single cell was employed to compute the total number of A3G(−) and A3G(+) viruses. The multi-scale system allowed us to achieve a quantitative understanding of the Vif-A3G pathway in HIV pathogenesis. Experimental data were used to establish system parameters such as stoichiometry of molecules, degradation rates of proteins, production profiles of viral proteins, viral burst size, cell proliferation rate, life-span of infected cells, viral generation time and virus clearance rate. We validated our system by reproducing the results of *in vitro* T cell culture experiments. We found that both downstream effects of A3G (hypermutation and reduction of viral burst size) were important to replicate the experimental results *in silico*. Based on the model simulations, *in vitro* virus clearance was estimated to be 24 hours.
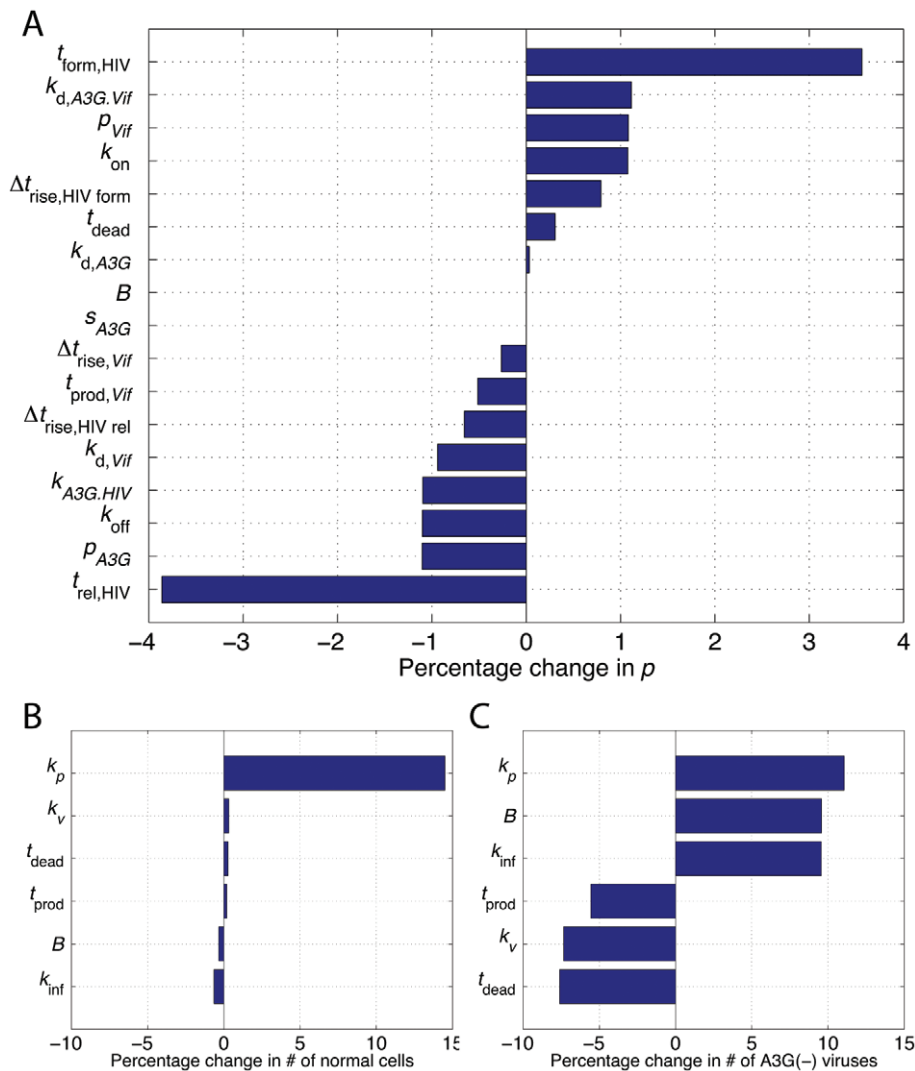
Figure 11. Sensitivity analysis in single-cell and multicellular models. (A) The values of all 17 parameters in the intracellular model have changed by +5% and the percentage change in p for each of them is shown. Two parameters representing the time origins of virus release and particle formation had the highest impact on p. In contrast, parameters such as burst size, the degradation rate of A3G, and the stoichiometry of A3G proteins incorporated in HIV particles had zero or negligible effects on p. For the extracellular model, the effects of parameter variations were studied on two outputs; (B) number of normal cells and (C) number of A3G(−) viruses on the 6th day. In both cases, variations of cells proliferation rate had the highest impact on the extracellular model outputs.
doi:10.1371/journal.pcbi.1002371.g011

The model also predicted that the average number of HIV viruses produced by an infected cell is 1900. We simulated two types of T cell cultures with unconstrained or constrained proliferation rate (including crowding effects by using a logistic function). It was observed that simulated HIV growth curves provided better fits to the experimental data in the latter case suggesting that proliferation may slow down in cell culture after it gets crowded.

Several therapeutic molecules targeting the Vif-A3G pathway were tested in our system. These included a high-affinity antibody to Vif [85], APOBEC3G itself, a mutated A3G with lower Vif-induced degradation rate (A3G$^{\Delta Ub}$) [88], and a mutated A3G that does not bind Vif (A3G$^{\Delta Vif}$) [89,90]. It was found that A3G$^{\Delta Vif}$ was the most effective drug that could stop HIV replication. This also implied that inhibition of A3G binding to Vif is a crucial step in blocking HIV replication. We further studied A3G$^{\Delta Vif}$ with respect to effects of penetrance and administration time on HIV replication. The model predicted that the drug must be available to almost 100% of the cells in order to get the desired efficacy. Also

it must be available to the cells shortly after inoculation in order for the cells to survive.

Sensitivity analysis of the single-cell and multicellular models helped us characterize parameters with significant impacts on the system. We did a local sensitivity analysis by changing each parameter by 5% and study their effects on the output parameters. In the single-cell model, we chose HIV replicative potential, the ratio of released A3G(−) viruses to the total number of released viruses, as the output parameter. This is a critical parameter in our system linking the two models together. We found that $t_{rel,HIV}$ and $t_{form,HIV}$ are the most sensitive parameters. This implies that slowing the assembly and budding process of HIV particles from the cells reduces the number of output A3G(−) viruses. In the multicellular model, two outputs were chosen for sensitivity analysis: 1) number of healthy cells and 2) number of A3G(−) viruses on the 6th day. We found that the proliferation rate of cells had the highest combined impact on both output parameters.

In this study, we primarily focused on molecular and cellular processes of HIV infection *in vitro*, however, this provides the necessary requirements to expand the model and move towards *in vivo* computation modeling of HIV. In the extended model, virus clearance *in vivo* and the mechanisms of cell birth, proliferation, and death would be different and new topics such as latency would come into play. Also, CD4+ T cells in the immune system can function as memory cells. Therefore, they can latently carry integrated HIV for the duration of their lifetime. These cells can survive for years and possibly decades and upon withdrawal of antiretroviral therapy, they become active and HIV viral loads rebound quickly. So, this concept of latency stage should also be accounted for in the model by having a small population of dormant infected cells that live for a long period of time and infrequently become activated to produce HIV. In addition, the immune system is also hugely diverse and has many more cells than *in vitro* cell culture experiments. Also, some tissues such as GI tract are more susceptible to HIV infection than others. Therefore, compartmentalization is essential and specific models need to be developed for each tissue and they must be closely linked to represent the whole body. The *in vivo* model will be more complicated but can answer some more fundamental questions about HIV pathogenesis than we can not cover with *in vitro* modeling.

References

1. Chiu YL, Greene WC (2008) The APOBEC3 cytidine deaminases: an innate defensive network opposing exogenous retroviruses and endogenous retro-elements. Annu Rev Immunol 26: 317–353.
2. Malim MH (2009) APOBEC proteins and intrinsic resistance to HIV-1 infection. Philos Trans R Soc Lond B Biol Sci 364: 675–687.
3. Goila-Gaur R, Strebel K (2008) HIV-1 Vif, APOBEC, and Intrinsic Immunity. Retrovirology 5: 51.
4. Albin JS, Harris RS (2010) Interactions of host APOBEC3 restriction factors with HIV-1 in vivo: implications for therapeutics. Expert Rev Mol Med 12: e4.
5. Strebel K, Luban J, Jeang K-T (2009) Human cellular restriction factors that target HIV-1 replication. BMC Med 7: 48.
6. Hultquist JF, Harris RS (2009) Leveraging APOBEC3 proteins to alter the HIV mutation rate and combat AIDS. Future Virol 4: 605.
7. Harris RS, Bishop KN, Sheehy AM, Craig HM, Petersen-Mahrt SK, et al. (2003) DNA Deamination Mediates Innate Immunity to Retroviral Infection. Cell 113: 803–809.
8. Mangeat B, Turelli P, Caron G, Friedli M, Perrin L, et al. (2003) Broad antiretroviral defence by human APOBEC3G through lethal editing of nascent reverse transcripts. Nature 424: 99–103.
9. Zhang H, Yang B, Pomerantz RJ, Zhang C, Arunachalam SC, et al. (2003) The cytidine deaminase CEM15 induces hypermutation in newly synthesized HIV-1 DNA. Nature 424: 94–98.
10. Lecossier D, Bouchonnet F, Clavel F, Hance AJ (2003) Hypermutation of HIV-1 DNA in the Absence of the Vif Protein. Science 300: 1112.
11. Sheehy AM, Gaddis NC, Choi JD, Malim MH (2002) Isolation of a human gene that inhibits HIV-1 infection and is suppressed by the viral Vif protein. Nature 418: 646–650.
12. Mariani R, Chen D, Schröfelbauer B, Navarro F, König R, et al. (2003) Species-Specific Exclusion of APOBEC3G from HIV-1 Virions by Vif. Cell 114: 21–31.
13. Suspene R, Sommer P, Henry M, Ferris S, Guetard D, et al. (2004) APOBEC3G is a single-stranded DNA cytidine deaminase and functions independently of HIV reverse transcriptase. Nucl Acids Res 32: 2421–2429.
14. Harris RS, Sheehy AM, Craig HM, Malim MH, Neuberger MS (2003) DNA deamination: not just a trigger for antibody diversification but also a mechanism for defense against retroviruses. Nat Immunol 4: 641–643.
15. Yang B, Chen K, Zhang C, Huang S, Zhang H (2007) Virion-associated Uracil DNA Glycosylase-2 and Apurinic/Apyrimidinic Endonuclease Are Involved in the Degradation of APOBEC3G-edited Nascent HIV-1 DNA. J Biol Chem 282: 11667–11675.
16. Schumacher AJ, Hache G, MacDuff DA, Brown WL, Harris RS (2008) The DNA Deaminase Activity of Human APOBEC3G Is Required for Ty1, MusD, and Human Immunodeficiency Virus Type 1 Restriction. J Virol 82: 2652–2660.
17. Kaiser SM, Emerman M (2006) Uracil DNA Glycosylase Is Dispensable for Human Immunodeficiency Virus Type 1 Replication and Does Not Contribute to the Antiviral Effects of the Cytidine Deaminase Apobec3G. J Virol 80: 875–882.
18. Mbisa JL, Barr R, Thomas JA, Vandegraaff N, Dorweiler IJ, et al. (2007) HIV-1 cDNAs Produced in the Presence of APOBEC3G Exhibit Defects in Plus-Strand DNA Transfer and Integration. J Virol 81: 7099–7110.
19. Newman ENC, Holmes RK, Craig HM, Klein KC, Lingappa JR, et al. (2005) Antiviral Function of APOBEC3G Can Be Dissociated from Cytidine Deaminase Activity. Curr Biol 15: 166–170.
20. Bishop KN, Holmes RK, Malim MH (2006) Antiviral Potency of APOBEC Proteins Does Not Correlate with Cytidine Deamination. J Virol 80: 8450–8458.
21. Li X-Y, Guo F, Zhang L, Kleiman L, Cen S (2007) APOBEC3G Inhibits DNA Strand Transfer during HIV-1 Reverse Transcription. J Biol Chem 282: 32065–32074.
22. Bishop KN, Verma M, Kim E-Y, Wolinsky SM, Malim MH (2008) APOBEC3G Inhibits Elongation of HIV-1 Reverse Transcripts. PLoS Pathog 4: e1000231.
23. Iwatani Y, Chan DSB, Wang F, Maynard KS, Sugiura W, et al. (2007) Deaminase-independent inhibition of HIV-1 reverse transcription by APOBEC3G. Nucleic Acids Res 35: 7096–7108.
24. Guo F, Cen S, Niu M, Saadatmand J, Kleiman L (2006) Inhibition of Formula-Primed Reverse Transcription by Human APOBEC3G during Human Immunodeficiency Virus Type 1 Replication. J Virol 80: 11710–11722.
25. Guo F, Cen S, Niu M, Yang Y, Gorelick RJ, et al. (2007) The interaction of APOBEC3G with HIV-1 nucleocapsid inhibits tRNALys3 annealing to viral RNA. J Virol 81: 11322–11331.
26. Luo K, Wang T, Liu B, Tian C, Xiao Z, et al. (2007) Cytidine Deaminases APOBEC3G and APOBEC3F Interact with Human Immunodeficiency Virus Type 1 Integrase and Inhibit Proviral DNA Formation. J Virol 81: 7238–7248.
27. Miyagi E, Opi S, Takeuchi H, Khan M, Goila-Gaur R, et al. (2007) Enzymatically Active APOBEC3G Is Required for Efficient Inhibition of Human Immunodeficiency Virus Type 1. J Virol 81: 13346–13353.
28. Browne EP, Allers C, Landau NR (2009) Restriction of HIV-1 by APOBEC3G is cytidine deaminase-dependent. Virology 387: 313–321.
29. Schumacher AJ, Nissley DV, Harris RS (2005) APOBEC3G hypermutates genomic DNA and inhibits Ty1 retrotransposition in yeast. Proc Natl Acad Sci USA 102: 9854–9859.
30. von Schwedler U, Song J, Aiken C, Trono D (1993) Vif is crucial for human immunodeficiency virus type 1 proviral DNA synthesis in infected cells. J Virol 67: 4945–4955.
31. Sova P, Volsky DJ (1993) Efficiency of viral DNA synthesis during infection of permissive and nonpermissive cells with vif-negative human immunodeficiency virus type 1. J Virol 67: 6322–6326.
32. Simon J, Malim M (1996) The human immunodeficiency virus type 1 Vif protein modulates the postpenetration stability of viral nucleoprotein complexes. J Virol 70: 5297–5305.

Supporting Information

Figure S1 Comparison of model predictions using the two coupling methods. In all the simulations, 500,000 cells were inoculated by 1 ng 24 WT HIV input. $A3G_{\Delta Vif}$ with different production rates were administered right after inoculation. The red and blue lines represent $A3G(-)$ and $A3G(+)$ viruses in the culture, respectively. The green lines characterize all the viruses including $A3G(-)$, $A3G(+)$, and dead ones. Dashed lines represent cultures with constrained proliferation (crowding effects modeled by using a logistic function). The intracellular and multicellular model were coupled using either (A–D) equations (12a/b) or or (E–H) equations (11a/b). Although the coupling method using equations (11a/b) assumes that release rate of viruses from a productive cell (and the ratio of $A3G(-)$ to total viruses) is constant over the period [t_{prod}, t_{dead}], it provides a very good approximation of the model predictions obtained by the second coupling method using equations (12a/b). Note that there is no assumption on the rate of virus release in the second method and the actual time-dependent profile of virus release from a single cell is used to compute the total number of $A3G(-)$ and $A3G(+)$ viruses in culture supernatant.
(PDF)

Author Contributions

Conceived and designed the experiments: IH FMG. Performed the experiments: IH. Analyzed the data: IH FMG. Wrote the paper: IH FMG.

33. Chiu Y-L, Soros VB, Kreisberg JF, Stopak K, Yonemoto W, et al. (2005) Cellular APOBEC3G restricts HIV-1 infection in resting CD4+ T cells. Nature 435: 108–114.

34. Santoni de Sio FR, Trono D (2009) APOBEC3G-Depleted Resting CD4+ T Cells Remain Refractory to HIV1 Infection. PLoS One 4: e6571.

35. Kamata M, Nagaoka Y, Chen ISY (2009) Reassessing the Role of APOBEC3G in Human Immunodeficiency Virus Type 1 Infection of Quiescent CD4+ T-Cells. PLoS Pathog 5: e1000342.

36. Gramberg T, Sunseri N, Landau N (2009) Accessories to the crime: Recent advances in HIV accessory protein biology. Curr HIV/AIDS Rep 6: 36–42.

37. Malim MH, Emerman M (2008) HIV-1 Accessory Proteins–Ensuring Viral Survival in a Hostile Environment. Cell Host Microbe 3: 388–398.

38. Sheehy AM, Gaddis NC, Malim MH (2003) The antiretroviral enzyme APOBEC3G is degraded by the proteasome in response to HIV-1 Vif. Nat Med 9: 1404–1407.

39. Mehle A, Strack B, Ancuta P, Zhang C, McPike M, et al. (2004) Vif Overcomes the Innate Antiviral Activity of APOBEC3G by Promoting Its Degradation in the Ubiquitin-Proteasome Pathway. J Biol Chem 279: 7792–7798.

40. Marin M, Rose KM, Kozak SL, Kabat D (2003) HIV-1 Vif protein binds the editing enzyme APOBEC3G and induces its degradation. Nat Med 9: 1398–1403.

41. Stopak K, de Noronha C, Yonemoto W, Greene WC (2003) HIV-1 Vif Blocks the Antiviral Activity of APOBEC3G by Impairing Both Its Translation and Intracellular Stability. Mol Cell 12: 591–601.

42. Wang Y, Shao Q, Yu X, Kong W, Hildreth JEK, et al. (2011) N-Terminal Hemagglutinin Tag Renders Lysine-Deficient APOBEC3G Resistant to HIV-1 Vif-Induced Degradation by Reduced Polyubiquitination. J Virol 85: 4510–4519.

43. Kao S, Khan MA, Miyagi E, Plishka R, Buckler-White A, et al. (2003) The Human Immunodeficiency Virus Type 1 Vif Protein Reduces Intracellular Expression and Inhibits Packaging of APOBEC3G (CEM15), a Cellular Inhibitor of Virus Infectivity. J Virol 77: 11398–11407.

44. Schröfelbauer B, Chen D, Landau NR (2004) A single amino acid of APOBEC3G controls its species-specific interaction with virion infectivity factor (Vif). Proc Natl Acad Sci USA 101: 3927–3932.

45. Bogerd HP, Doehle BP, Wiegand HL, Cullen BR (2004) A single amino acid difference in the host APOBEC3G protein controls the primate species specificity of HIV type 1 virion infectivity factor. Proc Natl Acad Sci USA 101: 3770–3774.

46. Huthoff H, Malim MH (2007) Identification of amino acid residues in APOBEC3G required for regulation by human immunodeficiency virus type 1 Vif and virion encapsidation. J Virol 81: 3807–3815.

47. Zhang K-L, Mangeat B, Ortiz M, Zoete V, Trono D, et al. (2007) Model Structure of Human APOBEC3G. PLoS One 2: e378.

48. Khan M, Goila-Gaur R, Kao S, Miyagi E, Walker R, et al. (2009) Encapsidation of APOBEC3G into HIV-1 virions involves lipid raft association and does not correlate with APOBEC3G oligomerization. Retrovirology 6: 99.

49. Nowak MA, May R (2001) Virus dynamics: Mathematical principles of immunology and virology. New York: Oxford University Press.

50. Wodarz D, Nowak MA (2002) Mathematical models of HIV pathogenesis and treatment. BioEssays 24: 1178–1187.

51. Sedaghat AR, Dinoso JB, Shen L, Wilke CO, Siliciano RF (2008) Decay dynamics of HIV-1 depend on the inhibited stages of the viral life cycle. Proc Natl Acad Sci USA 105: 4832–4837.

52. Perelson AS (2002) Modelling viral and immune system dynamics. Nat Rev Immunol 2: 28–36.

53. Perelson AS, Neumann AU, Markowitz M, Leonard JM, Ho DD (1996) HIV-1 Dynamics in Vivo: Virion Clearance Rate, Infected Cell Life-Span, and Viral Generation Time. Science 271: 1582–1586.

54. Strain MC, Richman DD, Wong JK, Levine H (2002) Spatiotemporal Dynamics of HIV Propagation. J Theor Biol 218: 85–96.

55. Sedaghat AR, Siliciano RF, Wilke CO (2009) Constraints on the dominant mechanism for HIV viral dynamics in patients on raltegravir. Antivir Ther 14: 263–271.

56. Speirs C, van Nimwegen E, Bolton D, Zavolan M, Duvall M, et al. (2005) Analysis of Human Immunodeficiency Virus Cytopathicity by Using a New Method for Quantitating Viral Dynamics in Cell Culture. J Virol 79: 4025–4032.

57. Reddy B, Yin J (1999) Quantitative intracellular kinetics of HIV type 1. AIDS Res Hum Retroviruses 15: 273–283.

58. Zarrabi N, Mancini E, Tay J, Shahand S, Sloot PMA (2010) Modeling HIV-1 intracellular replication: two simulation approaches. Procedia Comput Sci 1: 555–564.

59. Haseltine EL, Rawlings JB, Yin J (2005) Dynamics of viral infections: incorporating both the intracellular and extracellular levels. Comput Chem Eng 29: 675–686.

60. Benedict K, Mac Gabhann F, Amanfu R, Chavali A, Gianchandani E, et al. (2011) Systems Analysis of Small Signaling Modules Relevant to Eight Human Diseases. Ann Biomed Eng 39: 621–635.

61. Arnold E, Sarafianos SG (2008) Molecular biology: An HIV secret uncovered. Nature 453: 169–170.

62. Arhel N (2010) Revisiting HIV-1 uncoating. Retrovirology 7: 96.

63. Marodon G, Warren D, Filomio MC, Posnett DN (1999) Productive infection of double-negative T cells with HIV in vivo. Proc Natl Acad Sci USA 96: 11958–11963.

64. Goila-Gaur R, Khan MA, Miyagi E, Kao S, Opi S, et al. (2008) HIV-1 Vif promotes the formation of high molecular mass APOBEC3G complexes. Virology 372: 136–146.

65. Dang Y, Siew LM, Zheng Y-H (2008) APOBEC3G Is Degraded by the Proteasomal Pathway in a Vif-dependent Manner without Being Polyubiquitylated. J Biol Chem 283: 13124–13131.

66. Auclair J, Somasundaran M, Schiffer C (2005) Low Resolution Structural Mapping of HIV-1 Vif and its Interaction with APOBEC3G. 3rd International AIDS Society Conference on HIV Pathogenesis and Treatment.

67. Xu H, Chertova E, Chen J, Ott DE, Roser JD, et al. (2007) Stoichiometry of the antiviral protein APOBEC3G in HIV-1 virions. Virology 360: 247–256.

68. van 't Wout AB, Lehrman GK, Mikheeva SA, O'Keeffe GC, Katze MG, et al. (2003) Cellular Gene Expression upon Human Immunodeficiency Virus Type 1 Infection of CD4+-T-Cell Lines. J Virol 77: 1392–1402.

69. Kim SY, Byrn R, Groopman J, Baltimore D (1989) Temporal aspects of DNA and RNA synthesis during human immunodeficiency virus infection: evidence for differential gene expression. J Virol 63: 3708–3713.

70. Schupbach J (2002) Measurement of HIV-1 p24 antigen by signal-amplification-boosted ELISA of heat-denatured plasma is a simple and inexpensive alternative to tests for viral RNA. AIDS Rev 4: 83–92.

71. Chono H, Matsumoto K, Tsuda H, Saito N, Lee K, et al. (2011) Acquisition of HIV-1 Resistance in T Lymphocytes Using an ACA-Specific E. coli mRNA Interferase. Hum Gene Ther 22: 35–43.

72. Sullenger BA, Gallardo HF, Ungers GE, Gilboa E (1991) Analysis of trans-acting response decoy RNA-mediated inhibition of human immunodeficiency virus type 1 transactivation. J Virol 65: 6811–6816.

73. Dimitrov DS, Willey RL, Sato H, Chang LJ, Blumenthal R, et al. (1993) Quantitation of human immunodeficiency virus type 1 infection kinetics. J Virol 67: 2182–2190.

74. Eckstein DA, Penn ML, Korin YD, Scripture-Adams DD, Zack JA, et al. (2001) HIV-1 Actively Replicates in Naive CD4+ T Cells Residing within Human Lymphoid Tissues. Immunity 15: 671–682.

75. Chun T-W, Carruth L, Finzi D, Shen X, DiGiuseppe JA, et al. (1997) Quantification of latent tissue reservoirs and total body viral load in HIV-1 infection. Nature 387: 183–188.

76. Haase AT, Henry K, Zupancic M, Sedgewick G, Faust RA, et al. (1996) Quantitative Image Analysis of HIV-1 Infection in Lymphoid Tissue. Science 274: 985–989.

77. Hockett RD, Kilby JM, Derdeyn CA, Saag MS, Sillers M, et al. (1999) Constant mean viral copy number per infected cell in tissues regardless of high, low, or undetectable plasma HIV RNA. J Exp Med 189: 1545–1554.

78. Chen HY, Di Mascio M, Perelson AS, Ho DD, Zhang L (2007) Determination of virus burst size in vivo using a single-cycle SIV in rhesus macaques. Proc Natl Acad Sci USA 104: 19079–19084.

79. Reilly C, Wietgrefe S, Sedgewick G, Haase A (2007) Determination of simian immunodeficiency virus production by infected activated and resting cells. AIDS 21: 163–168.

80. Ramratnam B, Bonhoeffer S, Binley J, Hurley A, Zhang L, et al. (1999) Rapid production and clearance of HIV-1 and hepatitis C virus assessed by large volume plasma apheresis. Lancet 354: 1782–1785.

81. Ho DD, Neumann AU, Perelson AS, Chen W, Leonard JM, et al. (1995) Rapid turnover of plasma virions and CD4 lymphocytes in HIV-1 infection. Nature 373: 123–126.

82. Wei X, Ghosh SK, Taylor ME, Johnson VA, Emini EA, et al. (1995) Viral dynamics in human immunodeficiency virus type 1 infection. Nature 373: 117–122.

83. Cen S, Peng Z-G, Li X-Y, Li Z-R, Ma J, et al. (2010) Small Molecular Compounds Inhibit HIV-1 Replication through Specifically Stabilizing APOBEC3G. J Biol Chem 285: 16546–16552.

84. Nathans R, Cao H, Sharova N, Ali A, Sharkey M, et al. (2008) Small-molecule inhibition of HIV-1 Vif. Nat Biotech 26: 1187–1192.

85. Jeffrey Fessel W (2005) A new approach to an AIDS vaccine: creating antibodies to HIV vif will enable apobec3G to turn HIV-infection into a benign problem. Med Hypotheses 64: 261–263.

86. Stopak KS, Chiu Y-L, Kropp J, Grant RM, Greene WC (2007) Distinct Patterns of Cytokine Regulation of APOBEC3G Expression and Activity in Primary Lymphocytes, Macrophages, and Dendritic Cells. J Biol Chem 282: 3539–3546.

87. Farrow MA, Kim E-Y, Wolinsky SM, Sheehy AM (2011) NFAT and IRF Proteins Regulate Transcription of the Anti-HIV Gene, APOBEC3G. J Biol Chem 286: 2567–2577.

88. Opi S, Kao S, Goila-Gaur R, Khan MA, Miyagi E, et al. (2007) Human immunodeficiency virus type 1 Vif inhibits packaging and antiviral activity of a degradation-resistant APOBEC3G variant. J Virol 81: 8236–8246.

89. Russell RA, Smith J, Barr R, Bhattacharyya D, Pathak VK (2009) Distinct domains within APOBEC3G and APOBEC3F interact with separate regions of human immunodeficiency virus type 1 Vif. J Virol 83: 1992–2003.

90. Mangeat B, Turelli P, Liao S, Trono D (2004) A single amino acid determinant governs the species-specific sensitivity of APOBEC3G to Vif action. J Biol Chem 279: 14481–14483.